Carbon Neutrality

REVIEW Open Access

Strategies and reaction systems for solar-driven CO_2 reduction by water

Ji Bian[1], Ziqing Zhang[1], Ye Liu[1], Enqi Chen[2], Junwang Tang[2*] and Liqiang Jing[1*]

Abstract

Solar driven CO_2 conversion into high-value-added chemicals and energy-rich fuels is one of the promising strategies to tackle global warming and to address the energy-supply crisis. Even though enormous effort has been devoted to exploring all sorts of homogeneous and heterogeneous photocatalysts, the current efficiency and more importantly selectivity to valuable chemicals are still rather moderate, thus it is desired to develop high-efficiency photocatalytic system toward CO_2 reduction with excellent selectivity. In this review, fundamental aspects of photocatalytic CO_2 reduction by pure water, the reaction systems and the reliable method for detection of the products are firstly described. Thereafter the recent advances of the main strategy for improving the photocatalytic CO_2 reduction from the perspective of promoting the CO_2 adsorption and activation, accelerating the kinetics of water oxidation, and modulating charge separation are overviewed. The prospects and challenges on precise designing heterogeneous catalysts for CO_2 photoreduction are proposed at the end, indicating the significance for the further development of photocatalytic systems with high CO_2 conversion efficiency and product selectivity.

Keywords: Photocatalysis, CO_2 reduction, Selectivity, Water, Solar fuel production

1 Introduction

With the fast development of industrialization and rapid population growth, there is an ever-growing demand for energy consumption worldwide. Nowadays, 80 ~ 90% global energy consumption depends on the combustion of fossil fuels, which causes excessive carbon dioxide (CO_2) emission to the atmosphere and gives rise to global warming [1]. The latest data shows that global warming has increased dramatically during the past two decades, and the current global average temperature is 1.1 °C higher than that in the end of the nineteenth century [2]. That means human beings will face grim environmental and anthropological issues if anthropogenic CO_2 emission could not be effectively controlled and minimized. Thankfully, the global warming has aroused the public concerns and it is imperative to drastically reduce CO_2 emission. Numerous efforts have been devoted to replacing fossil fuels with renewable energy (solar, wave, wind, and biomass, etc.) and developing effective technologies for sustainable energy production [3, 4]. Representative water splitting and CO_2 reduction driven by inexhaustible solar energy are attractive approaches to energy conversion. As for photocatalytic water splitting, it is a relatively simple reaction with water as the only reactant. In particular overall water splitting has been considered as a cost-effective technology to scale up solar hydrogen production with the merits of ready synthesis of the reasonably priced photocatalyst along with the simple reactor and equipment designs.

Turning to CO_2 reduction, various technologies have been developed to convert CO_2 into carbonaceous fuels, such as electrocatalysis, thermocatalysis, and photocatalysis, etc. [5–7]. In particular, the transformation of CO_2 into chemical fuels with photovoltaic-powered electrochemical reduction and photoreduction are appealing in varieties of feasible strategies, since these two avenues could be achieved in normal pressure and temperature,

* Correspondence: Junwang.tang@ucl.ac.uk; jinglq@hlju.edu.cn
[2]Department of Chemical Engineering, University College London Torrington Place, WC1E 7JE, London, UK
[1]Department Key Laboratory of Functional Inorganic Materials Chemistry (Ministry of Education), International Joint Research Center and Lab for Catalytic Technology, School of Chemistry and Materials Science, Heilongjiang University, Harbin 150080, People's Republic of China

and the required energy can be directly or indirectly provided by solar energy to truly realize carbon recycling [8, 9]. Photovoltaic-powered electrochemical reduction of CO_2 is driven by photovoltaic cells to generate sufficient photovoltage and then supplied to the cathode for CO_2 reduction and the anode for water oxidation. In this case, the design of photovoltaic and the employed electrocatalysts are flexible, which could be optimized individually and then assembled together to access the best overall performance. While the products selectivity and poor stability of electrocatalyst are still the obstacles to the development of electrocatalytic CO_2 reduction. In contrast, the wireless configuration of photocatalytic CO_2 reduction endows the device design much more facile and compact. Moreover, it could utilize the enormous solar energy directly, which is a competitive approach with the merits of nonpollution, inexhaustibility, and nonenergy inputs for energy conversion. In addition, the products selectivity could be ingeniously modulated from the perspective of energy band structures of photocatalysts, adsorption/activation of reactants, surface active sites as well as the adsorption/desorption of intermediates, and the desired hydrocarbons could be accessed based on the above considerations. This is more competitive than the electrochemical reduction pathway since most CO_2 reduction electrocatalysts yield CO or formate as the primary reduction products.

Since the first case that Inoue et al. realized the CO_2 photoreduction in the aqueous system [10], the photocatalytic CO_2 reduction field has witnessed a dramatic expansion in research directed at photocatalytic systems. There have been explored varieties of photocatalysts for CO_2 reduction in recent decades, including homogeneous catalysts as well as heterogeneous ones (Table 1). Of course, the activity and the selectivity of photocatalysts are closely related with the reaction media. An ideal photocatalytic CO_2 conversion system is similar to the natural photosynthesis of green plants which can exploit the energy of incident photons to convert CO_2 and H_2O into carbohydrates and O_2. That is to say, the photocatalysts are excited by photons and generate pairs of electrons and holes to reduce CO_2 with protons and oxidize H_2O, respectively [11]. However, many reported photocatalysts could not simultaneously accomplish the CO_2 reduction and H_2O oxidation, and thus the organic hole scavengers, for example, triethanolamine (TEOA), trimethylamine (TEA), and ethylenediaminetetraacetic acid (EDTA), were used in CO_2 photoreduction as electron/proton donors [12, 13], especially for some metal-organic framework (MOF) materials and metal sulfide semiconductors [14–18]. Such photocatalytic CO_2 reduction systems sacrifices expensive electron/proton donors instead of H_2O oxidation half-reaction which is unsustainable and uneconomical. In addition, the photocatalytic CO_2 reduction reaction is a complex multistep process, and the stoichiometric CO_2 reduction and H_2O oxidation is of great significance to deeply understand the reaction mechanism and tune product selectivity. While the H_2 evolution reaction (HER) usually becomes an observable competitive process in the presence of water, which possibly leads to low efficiency of CO_2 photoreduction [19]. Therefore, it is a grand challenge on smart design and fabrication of efficient photocatalytic systems for CO_2 reduction coupled with pure water oxidation.

From a thermodynamic point of view, the photocatalytic system must satisfy the reduction potentials of CO_2, and simultaneously maintain a high redox potential for the oxidation of H_2O to O_2. Besides, more attention should be paid to the CO_2 adsorption and activation, which is extremely important for inhibiting HER reactions and determining the CO_2 reduction reaction pathways. From a dynamic perspective, the water oxidation by holes proceeds at < s timescale [43], which is unambiguous to be the rate-determining step in overall CO_2 photoreduction process. Accordingly, the modulation and acceleration of photogenerated hole to initiate the surface oxidation reaction are critical to the conversion efficiency in water without the usage of any sacrificial agent. In addition, it should be noted that the recombination of photogenerated electron-hole pairs from the excited semiconductors occurs at < μs timescale, which is much faster than the water oxidation by holes [20, 29, 31, 44–46]. Therefore, strategies should be developed to enhance the charge separation, especially for the spatial charge separation, with efforts to achieving efficient CO_2 photoreduction.

Up to now, there have been many reviews focusing on the design and fabrication of various semiconductor photocatalysts, as well as the complex process of photocatalytic CO_2 reduction reaction [9, 47]. To differentiate from these review articles, we try to make an interesting review from the perspective of coupling CO_2 reduction with pure water oxidation. Firstly, the basic principle and procedure of photocatalytic CO_2 reduction coupled H_2O oxidation are discussed in detail. Then, the current widely-used reaction systems and products detection are comprehensively summarized. Special emphases are given on the strategies for improving photocatalytic CO_2 reduction performance, including co-catalysts engineering for CO_2 adsorption and activation, accelerating the kinetics of water oxidation, and promoting charge separation by constructing Z-scheme heterojunctions. Finally, the conclusions, challenges and perspectives concerning on efficient heterogeneous photocatalytic systems for CO_2 reduction with H_2O are presented.

Table 1 Representative summary of photocatalytic CO_2 reduction systems

Catalyst	Light source	Photosensitizer	Reaction media	Major products	Selectivity	Activity	Ref.
^{m}CD/CN	Visible light	-	H_2O	CH_3OH	99.6%	13.9 μmol g^{-1} h^{-1}	Tang et al. 2020 [20]
MXene/Bi_2WO_6	UV-Vis light	-	H_2O, $NaHCO_3$, H_2SO_4	CH_4 CH_3OH	-	1.78 μmol g^{-1} h^{-1} 0.44 μmol g^{-1} h^{-1}	Yu et al. 2020 [21]
Cu_2O@$Cu_3(BTC)_2$	Visible light	-	H_2O vapor	CH_4	100%	0.73 mmol (8 h)	Tang et al. 2021 [22]
Ni-SA-x/ZrO_2	UV-vis light	-	H_2O	CO	92.5%	11.8 μmol g^{-1} h^{-1}	Zhang et al. 2020 [23]
CuPc/g-C_3N_4	Visible light	-	H_2O	CO CH_4	-	1.5 μmol g^{-1} h^{-1}	Jing et al. 2020 [24]
Mn, C-ZnO CTSHS	UV-vis light	-	H_2O	CO		0.83 μmol g^{-1}	Yu et al. 2021 [25]
CD/FAT	Visible light	-	H_2O	CH_3OH	100%	24.2 μmol g^{-1} h^{-1}	Tang et al. 2021 [26]
NiMn–COS–UCN	UV-vis light	-	H_2O	CO CH_4	-	13.85 μmol g^{-1} h^{-1} 2.22 μmol g^{-1} h^{-1}	Jing et al. 2021 [27]
1Au-6T/0.8M/PCN	Visible light	-	H_2O	CH_4		140 μmol g^{-1} h^{-1}	Jing et al. 2018 [28]
$BiVO_4${010}–Au–Cu_2O	Visible light	-	H_2O	CO CH_4	-	2.02 μmol g^{-1} h^{-1} 3.14 μmol g^{-1} h^{-1}	Zhou et al. 2018 [18]
$SrTiO_3$:La, Rh|Au|RuO_2-$BiVO_4$:Mo	Visible light	-	H_2O, $KHCO_3$	$HCOO^-$ CO	97%	6.53 μmol g^{-1} h^{-1}	Demon et al. 2020 [29]
(001)TiO_2-g-C_3N_4/$BiVO_4$	Visible light	-	H_2O	CO CH_4	-	5.18 μmol g^{-1} h^{-1}	Jing et al. 2021 [30]
Cu_2O-Pt/SiC/IrOx	Visible light	-	H_2O, $FeCl_3$	HCOOH	-	896.7 μmol g^{-1} h^{-1}	Li et al. 2020 [31]
COF-318-TiO_2	Visible light	-	H_2O	CO	-	69.67 μmol g^{-1} h^{-1}	Lan et al. 2020 [32]
ZnPc/BVNS	Visible light	-	H_2O	CO CH_4	-	0.97 μmol g^{-1} h^{-1}	Jing et al. 2019 [33]
TiO_2/C_3N_4/Ti_3C_2 Mxene	UV-vis light	-	H_2O, H_2SO_4, $NaHCO_3$,	CO CH_4	-	4.39 μmol g^{-1} h^{-1} 1.20 μmol g^{-1} h^{-1}	Yu et al. 202 [34]
$[PMo^{V}_{8}Mo^{VI}_{4}O_{35}(OH)_5Zn_4]_2$ [Zn-TCPP][$2H_2O$]·xGuest(NNU-13)	Visible light	-	H_2O, TEOA	CH_4	96.6%	117 μmol g^{-1} h^{-1}	Lan et al. 2020 [35]
$W_{18}O_{49}$@Co	Visible light	$Ru(bpy)_3^{2+}$	H_2O, MeCN, TEOA	CO	-	21.18 mmol g^{-1} h^{-1}	Lou et al. 2021 [36]
IrQPY/CoPc	Visible light	Ir Ps	CH_3CN, BIH, TEA	CO	98%	-	Ouyang et al. 2021 [37]
3DOM CdSQD/NC	Visible light	$Co(bpy)_3^{2+}$	H_2O, MeCN, Benzylamine	CO	89.6%	5210 μmol g^{-1} h^{-1}	Wang et al. 2021 [38]
TiO_2/$CsPbBr_3$	Uv-Vis light	$Ru(bpy)_3^{2+}$	H_2O, MeCN, BIH	CO	-	9.02 μmol g^{-1} h^{-1}	Yu et al. 2020 [39]
$[Ni(tpy)_2]^{2+}$	Visible light	$Ru(bpy)_3^{2+}$	H_2O, CH_3CN, BIH	CO	99%	-	Xiong et al. 2019 [40]
NiCoOP-NPs@MHCFs	Visible light	$Ru(bpy)_3^{2+}$	H_2O, MeCN, TEOA	CO	-	16.6 μmol h^{-1}	Lou et al. 2019 [41]
Au/CdS-HMCHPs	Visible light	$Co(bpy)_3^{2+}$	H_2O, MeCN, TEOA	CO	70.3%	3758 μmol g^{-1} h^{-1}	Lou et al. 2019 [42]

2 Basic principle and procedure of photocatalytic CO_2 reduction

The basic principle of semiconductor photocatalysis is mainly based on energy band theory of solid-state physics. The band structure of a semiconductor is not successive, which consists of multiple energy bands, including the valence band (VB), the conduction band (CB), and the forbidden band. In general, the VB of a semiconductor is fully filled with valence electrons at low temperatures, while there are little electrons in the bottom of CB, in which most of the energy levels are unoccupied. There is a space between the top of the VB and the bottom of CB that electrons are unable to exist, which is denoted as the forbidden band. The energy difference between the CB and the VB is called bandgap. When a semiconductor photocatalyst absorbs photons with the energy equal to or greater than its bandgap, the electrons in the VB will be excited to the CB, while leaving the holes in the VB. The generated electrons and holes would further migrate to the surface of a semiconductor, and initiate the redox reactions with the adsorbed reactants on the surface. Meanwhile, a proportion of the electrons and holes would recombine in the bulk or on the surface of semiconductors through the electrostatic force [48]. Based on the fundamentals of photocatalysis, the procedure of CO_2 photoreduction by pure water is mainly involved with the following procedures:

(i) CO_2 adsorption. The CO_2 adsorption and activation play a crucial role in tuning the activity and selectivity of photocatalytic CO_2 conversion [49]. On one hand, if the photocatalyst surface is favorable for CO_2 adsorption, the photogenerated electrons would be more easily captured by CO_2 that adsorbed on the catalyst surface after being transferred from the bulk to the catalyst surface, which can reduce the recombination of photogenerated charge carriers to a certain extent, and improve the utilization efficiency of

photoelectrons [50]. On the other hand, CO_2 is a thermodynamically stable nonpolar molecular with linear configuration, and the bond energy of C=O (750 kJ mol^{-1}) is much higher than that of C – C (336 kJ mol^{-1}), C – O (327 kJ mol^{-1}) and C – H (411 kJ mol^{-1}) [11]. As a result, the photoreduction of CO_2 needs to overcome a higher activation energy to break the C=O bonds. It is understood that the adsorbed CO_2 could become a partially charged $CO_2^{\delta\bullet-}$ species via the interactions with surface atoms [51]. The adsorbate no longer has the initial linear symmetry of the free CO_2 molecule and thus lower the energy barriers for accepting an electron since the lowest unoccupied molecular orbital (LUMO) level of CO_2 decreases as the molecule bends [52]. Figure 1 shows the possible structures of adsorbed $CO_2^{\delta\bullet-}$ species on catalysts [53]. Moreover, the main adsorbed structure of CO_2 on the surface of a photocatalyst is determined by its chemical properties, which has a significant influence on the subsequent reaction pathways and selectivity.

(ii) Excitation and migration of photogenerated charge carriers. The electron-hole pairs generates when a photocatalysts absorb the incident photons with energy equal to or greater than the bandgap, and then the photogenerated electrons and holes migrate independently to the surface of a photocatalyst (Fig. 2). Since the recombination of charge carriers (~ 10^{-9} s) is considerably faster than the surface redox processes (10^{-3} to 10^{-8} s) [54, 55], it is always accompanied by the undesirable electron-hole recombination in bulk or on the surface of photocatalysts. As a result, the rapid migration of charge carrier from bulk to the surface could effectively restrain the electron-hole recombination, which enables more photogenerated charge carriers to participate in the subsequent redox reactions [56]. The quantity of the initial photogenerated charge carriers of semiconductor photocatalysts depends on the inherent bandgap, while the redox capacity of the charge carriers is determined by the energy band alignments. In general, the bottom of the CB of a photocatalyst has to be more negative than the CO_2 reduction potential and the corresponding reduction products, while the top of the VB of a photocatalyst has to be more positive than the potential of water oxidation.

(iii) Surface catalytic reactions with CO_2 and H_2O. The photocatalytic CO_2 reduction by water consist of two half reactions, namely, the electron-initiated CO_2 reduction reaction and the hole-induced water oxidation reaction. In general, one-electron transfer to form a $CO_2^{\bullet-}$ intermediate [Eq. (1)] is believed to be the first step to initiate a series of subsequent reactions. Whereas, the fairly negative thermodynamic potential of – 1.9 V versus NHE at pH=7 makes the candidate semiconductors impossible to directly drive such reactions by single-electron transfer[23]. Proton-assisted multiple-electron transfer turns to be an alternative and feasible route to reduce CO_2 via passing by the formation of $CO_2^{\bullet-}$ [Eqs. (2), (3), (4), (5), (6), (7), (8), (9) and (10)] [32, 57]. The activation barriers of CO_2 conversion decrease gradually with the merits of several electrons and protons simultaneously transferred in pairs to CO_2. According to the number of the involved electrons and protons transferred, CO_2 can be converted to C_1 compounds such as CO, CH_4, CHOH, HCOOH and CH_3OH as well as high-value-added hydrocarbons.

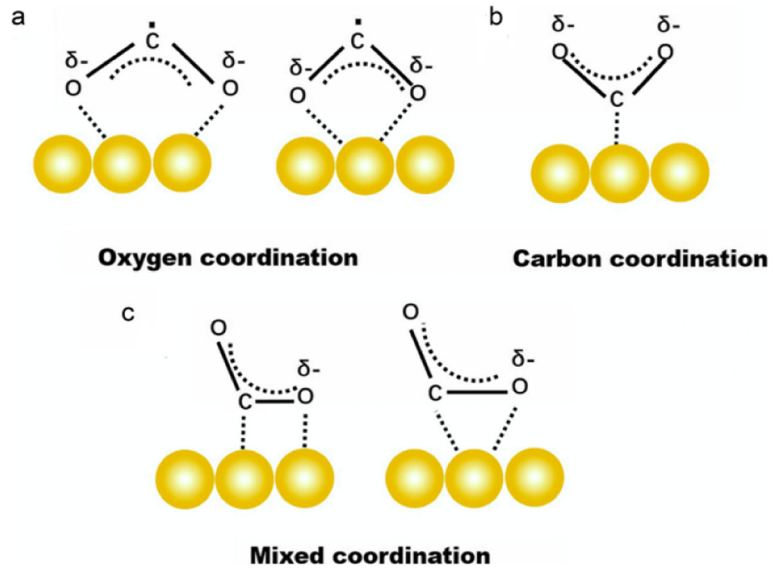

Fig. 1 The possible structures of adsorbed $CO_2^{\delta-}$ species on catalysts [53] Copyright 2020, Elsevier

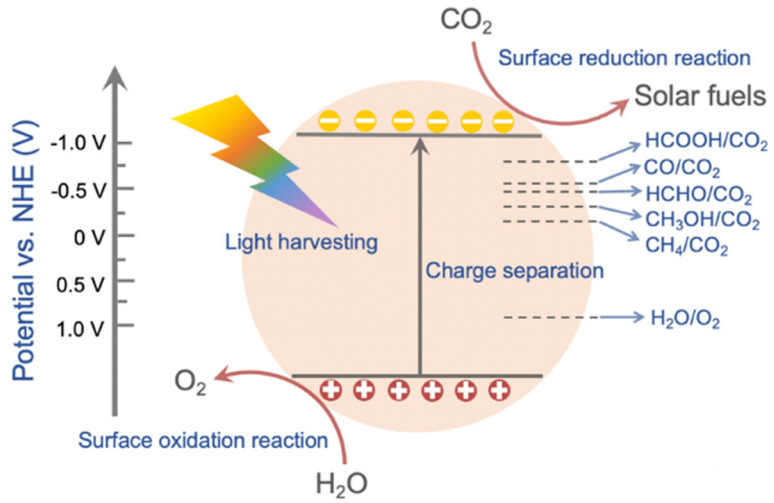

Fig. 2 Schematic illustration of photocatalytic CO_2 reduction by water over a photocatalyst at pH = 7

Of note, most studies on CO_2 photoreduction are focused on the reduction side, yet less attention has paid to the oxidation half-reaction. In principle, if the VB energy level of a semiconductor is positive than the redox potential of O_2/H_2O (0.81 V vs NHE), the photogenerated holes would react with the adsorbed H_2O or OH^-_{ads} on the surface of semiconductors to produce O_2 and H^+ [Eqs. (11)]. However, the formation of O_2 is relatively difficult due to the need for four holes per oxygen molecule and the challenge of its desorption. An alternative to the generation of oxygen is the formation of hydroxyl radicals with strong oxidizing [Eqs. (12)]. It is worth noting that the produced H^+ could participate in the CO_2 reduction reaction, as well as the competitive reaction of water reduction to H_2 [Eqs. (13)]. The oxidative environment complicates the CO_2 reduction pathway since some intermediate species would be more favorable to oxidize than reduce, as a result interrupting the process before the multiple-electron reduction products are obtained.

The related potentials for CO_2 conversion at pH = 7, vs NHE

$$CO_2g + e^- \rightarrow CO_2^{\cdot -} \quad E^\theta = -1.90\ V \tag{1}$$

$$CO_2(g) + 2H^+ + 2e^- \rightarrow CO(g) + H_20(l) \quad E^\theta = -0.53\,V \tag{2}$$

$$CO_2(g) + 8H^+ + 8e^- \rightarrow CH_4(g) + 2H_20(l) \quad E^\theta = -0.24\,V \tag{3}$$

$$CO_2(g) + 4H^+ + 4e^- \rightarrow HCHO(g) + 2H_20(l) \quad E^\theta = -0.48\,V \tag{4}$$

$$CO_2(g) + 2H^+ + 2e^+ \rightarrow HCOOH(l) \quad E^\theta = -0.61\,V \tag{5}$$

$$CO_2(g) + 6H^+ + 6e^- \rightarrow CH_3OH(l) \quad E^\theta = -0.38\,V \tag{6}$$

$$2CO_2(g) + 8H^+ + 8e^- \rightarrow CH_3COOH(l) + 2H_20(l) \quad E^\theta = -0.30\,V \tag{7}$$

$$2CO_2(g) + 12H^+ + 12e^- \rightarrow CH_3CH_2OH(l) + 3H_20(l) \quad E^\theta = -0.32\,V \tag{8}$$

$$2CO_2(g) + 12H^+ + 12e^- \rightarrow C_2H_4(g) + 4H_20(l) \quad E^\theta = -0.33\,V \tag{9}$$

$$2CO_2(g) + 14H^+ + 14e^- \rightarrow C_2H_6(g) + 4H_20(l) \quad E^\theta = -0.27\,V \tag{10}$$

$$2H_20(l) + 4h^+ \rightarrow 0_2(g) + 4H^+ \quad E^\theta = +0.81\,V \tag{11}$$

$$2H_20(l) + h^+ \rightarrow 0H + H^+ \quad E^\theta = +2.31\,V \tag{12}$$

$$2H^+ + 2e^- \rightarrow H_2(g) \quad E^\theta = -0.42\,V \tag{13}$$

(iv) *Desorption of the products.* The catalytic active site plays a crucial role in the final activity and selectivity of CO_2 reduction. If the products cannot be desorbed from the surface of a photocatalyst in time, the active site would be coated or poisoned that result in decreasing the reaction rate and ceasing the subsequent chemical reaction [9]. In the course of photocatalytic CO_2 reduction, varieties of intermediates could be obtained, and the interactions between intermediates and

photocatalysts have great influence on the yield and selectivity of CO_2 photoreduction. If the interaction was strong, the intermediates would be difficult to release from the surface of photocatalysts, and the subsequent hydrogenation reaction would be more likely occurred. On the contrary, if the binding energy of the intermediates on the surface of a photocatalyst is weak, the products desorption from the photocatalysts surface would be more likely performed, and the specific products would be preferentially produced.

3 Reaction systems and products detection for CO_2 reduction

3.1 Reaction systems

The photocatalytic CO_2 reduction requires suitable reactant, which could react with h^+ and simultaneously provide protons for CO_2 reduction. The categories and dosage of reactant have a significant impact on the activity and the selectivity of CO_2 reduction. Abundant water with the merits of low-cost, pro-environment, etc. has been appealing electron/proton donors to replace those sacrificial regents to achieve sustainable CO_2 reduction.

To date, there are two kinds of preoccupant photocatalytic CO_2 reduction systems with water as reducing agent, namely, the solid-liquid reaction system and the gas-solid reaction system. The schematic diagram of the devices for these two reaction systems are shown in Fig. 3. The former one contains the catalyst powder and water in a sealed reactor, and the reactor is evacuated or bubbled with N_2 or Ar, etc. inert gas to remove air dissolved in liquid, and then filled with saturated CO_2 by means of bubbling or injection before formal photoreduction reactions [58, 59]. Some studies also directly disperse the catalyst into $NaHCO_3$ or $KHCO_3$ solutions with a certain concentration for photocatalytic CO_2 reduction [60, 61]. Turning to the gas-solid reaction system, in which both CO_2 and water in the form of gas to participate in the reaction, while the catalyst is coated or directly dispersed in the reactor [20, 29, 31, 44–46, 54, 55]. In this case, CO_2 and H_2O vapor are produced by the reaction of $NaHCO_3$/$KHCO_3$ with acid solution, and their content are controlled by adjusting the reaction temperature and the concentration of reactant [62, 63]. It is worth noting that the reductive products are diverse in these two reaction systems. CH_3OH, CH_3CH_2OH, HCOOH and some other liquid products are dominant reductive products in the solid-liquid suspension system [6, 7, 20, 29, 31, 36, 44–46], while CO, CH_4, C_2H_4, C_2H_6 and other hydrocarbons with small chains are primary products in the solid-gas reaction system [26, 37, 38, 64–66]. Of note, the competitive H_2 evolution reaction from direct photocatalytic water reduction is an observable process, which seriously reduces the CO_2 conversion efficiency and hinder the selectivity of products [67]. Whereas, the impact of the undesirable H_2 evolution reaction on the efficiency and selectivity of CO_2 reduction is much weaker in the gas-solid reaction system due to the lower H_2O vapor content.

3.2 Products detection

3.2.1 Analysis of gaseous products

It is well acknowledged that the CO_2 reduction process involves multiple protons coupled electron reaction to produce a wide variety of products, such as H_2, CO, CH_4, CH_3OH, HCOOH, as well as even higher hydrocarbons. The analytical approaches are different in terms of the physical state of CO_2 reduction products. In general, the quantitative detection of gaseous products like CO, CH_4, HCHO and H_2 are analyzed by gas chromatograph equipped with a thermal conductivity detector (TCD) and/or flame ionization detector (FID). Thereinto, H_2 is detected by a TCD equipped with suitable capillary columns, for instance, TDX-01 columns, Molsieve 5 Å columns and so forth [68, 69]. While all organic substance including CH_4, HCHO and inorganic CO could be further detected by FID (Note: CO detection requires a methanation reactor which contains a Ni catalyst). The role of methanation reactor is to convert CO to CH_4 and then analyzed by the FID [20, 29, 31, 44–46]. In particular, in the water contained CO_2 reduction reaction, O_2 has been regarded as the major oxidative products. The detection of O_2 is significant for the confirmation of an overall CO_2 reduction reaction. The analytical method of O_2 is the same as H_2, which quantified by gas chromatograph equipped with a TCD. Definitely, prior to quantitative detection of the reaction products, a calibration using standard gas mixture with different concertation of the gas to be tested is indispensable [70].

3.2.2 Analysis of liquid products

In addition to gaseous products, the confirmation and detection of the potential liquid products in the course of photocatalytic CO_2 reduction are essential. HCOOH and CH_3OH are the most common liquid products. For instance, CH_3OH etc. small chain liquid products are usually taken from the reactor by syringe, and detected by gas chromatograph equipped with FID detector [26, 37, 38, 65, 71]. Other possible liquid products, such as HCOOH, is generally analyzed by high-performance liquid chromatography [72].

4 Strategies for improving photocatalytic performance of CO_2 reduction by water

4.1 Co-catalysts engineering for CO_2 adsorption and activation

Great efforts have been devoted to boost the photocatalytic activity of CO_2 reduction over the last decades, yet

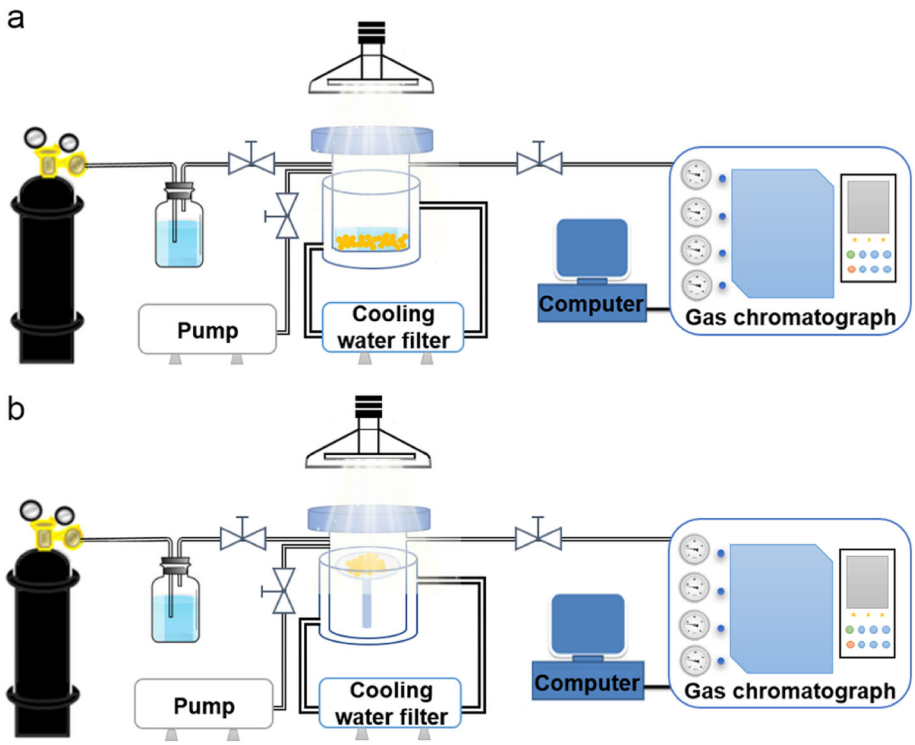

Fig. 3 Schematic diagram of the devices of the solid-liquid reaction system (**a**) and the gas-solid reaction system (**b**), respectively

the efficiency is still moderate due to the thermodynamically stable nature of CO_2. Typically, the initial step for CO_2 reduction is the adsorption process, and the linear configuration of CO_2 would become bent for the subsequent activation. Modification of cocatalysts on the photocatalysts could effectively lower the potential barrier for CO_2 activation, enhance the charge separation and simultaneously modulate the selectivity of the products, which has been a widely explored route to promote the photocatalytic activity of CO_2 reduction [73–75]. Developing low-cost, robust and sustainable cocatalysts to couple with photocatalysts as catalytic active sites, is prospected to greatly improve the photocatalytic activity.

Yu et al. reported a 2D/2D heterojunction of ultrathin Ti_3C_2/Bi_2WO_6 nanosheets for efficient CO_2 reduction, in which the Ti_3C_2 with abundant exposed metal sites served as an economical and stable cocatalyst [21]. The coupled Ti_3C_2 with several atomic layers remarkably promotes the CO_2 adsorption, and meanwhile the charge transport pathway in the Ti_3C_2/Bi_2WO_6 hybrid is greatly shortened, which is quite favorable for the transferred electrons from Bi_2WO_6 accumulated on the surface of Ti_3C_2 (Fig. 4a and b). Accordingly, the total yield of CH_4 and CH_3OH obtained on the optimal one is 4.6 times than that of pristine Bi_2WO_6 nanosheets. Very recently, Ng and Tang et al. developed a surfactant-free method to fabricate $Cu_2O@Cu_3(BTC)_2$ composite photocatalyst for selective CO_2 conversion (Fig. 4c) [22]. The coated $Cu_3(BTC)_2$ enlarges the surface area and increases CO_2 uptake, which offers a dense CO_2 atmosphere near the active catalytic sites. Importantly, the uncoordinated -COOH in Cu_3-$(BTC)_2$ framework that nearby the catalytic sites could form H-bonds with the intermediates of CO_2 reduction (*CO, *CHO, *CH_2O, and *OCH_3). Such interactions could prevent the desorption of the intermediates and lower the energy barrier for the CH_4 production, thus contributes to the selective evolution of CH_4 for $Cu_2O@Cu_3(BTC)_2$ composite.

Metal nanoparticle has been considered as an effective cocatalyst for photocatalytic reactions. The function of extracting photogenerated electrons and providing additional active sites makes it a promising candidate for CO_2 photoreduction. Despite there have some progress achieved on metal particle/semiconductor, it still confronts challenges of the efficiency and mechanism elucidation. The concept of single atom catalysis has triggered enormous attention and interest in recent years with the merits of maximum atom utilization efficiency, impressive catalytic activity, and unique selectivity. The isolated single atoms differ from traditional nanoparticles, because the former could fully expose the atomically dispersed metals and generated electrons and holes are easier to move to the surface of the catalyst. In this regard, scaling down the metal nanoparticles to single metal atoms affords great opportunity to maximize

metal atom utilization efficiency and to acquire uniform catalytic active sites [76]. Zhang et al. developed a simple strategy to dispersed isolated Ni single atoms on defect ZrO_2 for selective photocatalytic CO_2 conversion [23]. The crucial role of the atomically dispersed Ni sites has been systematically evidenced to lower the energy barrier for CO_2 to CO conversion via an adsorbed COOH intermediate (Fig. 5a and b). Meanwhile, it also suppressed H_2 desorption in the competitive water reduction reaction. Inspired by the single atom catalysis, the metal phthalocyanine (MPc) with the well-defined single atom metal sites that coordinated by four N atoms, has also been a potential single atom catalytic site for CO_2 conversion. Interestingly, the inherent M-N_4 sites of MPc with homogeneous configuration makes it more facile to be a uniform and stable isolate catalytic center than single atom sites, which needs to be precisely coordinated by N/C matrix (M-C/N unit). Jing's group designed an ultrathin CuPc/g-C_3N_4 heterojunction via a surface hydroxyl induced assembly process for CO_2 conversion [24]. It is worth noting that the coated CuPc served as a high-level-energy electron transfer platform, greatly prolonged the electron lifetime of g-C_3N_4, and the subsequent charge transfer from the ligand of CuPc to the center Cu-N_4 sites dramatically promotes the CO_2 adsorption and activation (Fig. 5c). In addition, this work emphasized that the controllable assembly of CuPc with high dispersion is crucial to expose abundant isolated catalytic active site for CO_2 concentration and conversion.

Actually, except the well acknowledged noble metals, transition metal-based materials, for instance, ions, oxides, sulfides and phosphides, etc. also exhibit appealing potentials for catalysis as cocatalysts. To date, it was found that most reported cocatalysts are in solid state. Very recently, a smart ionized cocatalyst has come into sight. Yu et al. proposed core-triple shell Mn, C-codoped ZnO hollow spheres as efficient photocatalysts for CO_2 conversion [25]. It was authenticated that the ionized Mn species could restore their primal oxidation state by means of capturing the photogenerated electrons from the CB of ZnO, which function as the active sites for CO_2 adsorption and activation. The embedded Mn ions with switchable valence states served as an "ionized cocatalyst" to provide electrons for CO_2 conversion. Interestingly, this process could be continuously operated due to the light-switchable valence state of Mn ions. Moreover, it turns out that CO is the predominant reduction products, and H_2 could be hardly detected, which might be correlated with the competitive H_2 evolution from water reduction is inhibited without noble metal cocatalysts.

4.2 Accelerated water oxidation kinetics

In an ideal photocatalytic CO_2 reduction reaction, the excited pairs of photogenerated electrons and holes would transfer to the surface of a semiconductor to reduce CO_2, and simultaneously to oxidize water to produce O_2. Even though continuous efforts have been devoted to the optimization of cocatalysts for CO_2 activation, it is often neglected that the water oxidation reaction which proceeds at seconds timescale is much slower than the undesirable electron-hole recombination (occurs at < μs time scale). Therefore, it is much meaningful to develop preferable semiconductors with long-lived charge carriers along with economical cocatalysts to extract photogenerated holes, so as to accelerate the water oxidation half reaction instead of charge recombination. Tang et al. ingeniously designed a unique hole-accepting carbon-dots decorated carbon nitride (^{m}CD/CN) for selective CO_2 reduction nearly 100% to methanol by pure water [20]. The ^{m}CD modification tackles the difficult water oxidation by greatly prolonging the lifetime of charge carriers to allow for electrons accumulation. In addition, it is evidenced that the ^{m}CD could selectively transfer holes towards H_2O rather than methanol. Significantly, the unique ^{m}CD as a hole acceptor in the ^{m}CD/CN has been clearly distinguished by

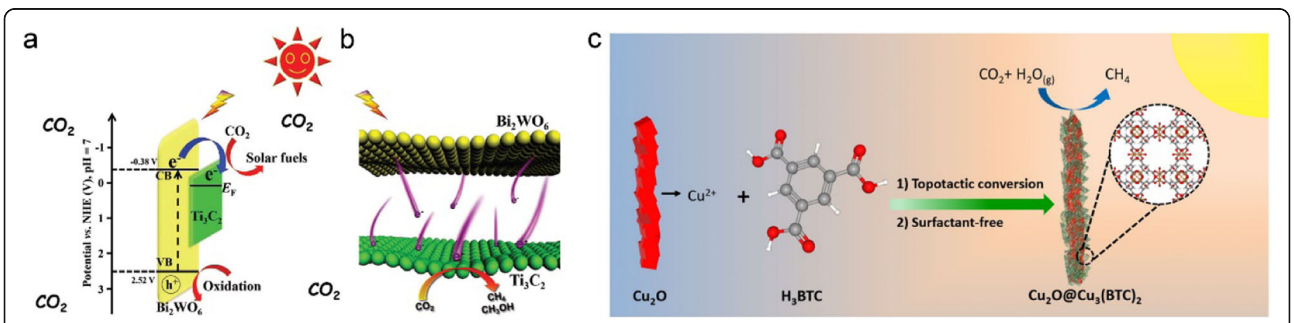

Fig. 4 (**a**) Energy level structure diagram of Bi_2WO_6 and Ti_3C_2 (**b**) Photo-induced electron transfer process at the interface of the hybrids [21] Copyright 2018, Wiley-VCH (**c**) Illustration of the synthetic route towards $Cu_2O@Cu_3(BTC)_2$ core–shell nanowires through a surfactant-free topotactic conversion strategy for selective photocatalytic carbon dioxide reduction to methane [22] Copyright 2021, Wiley-VCH

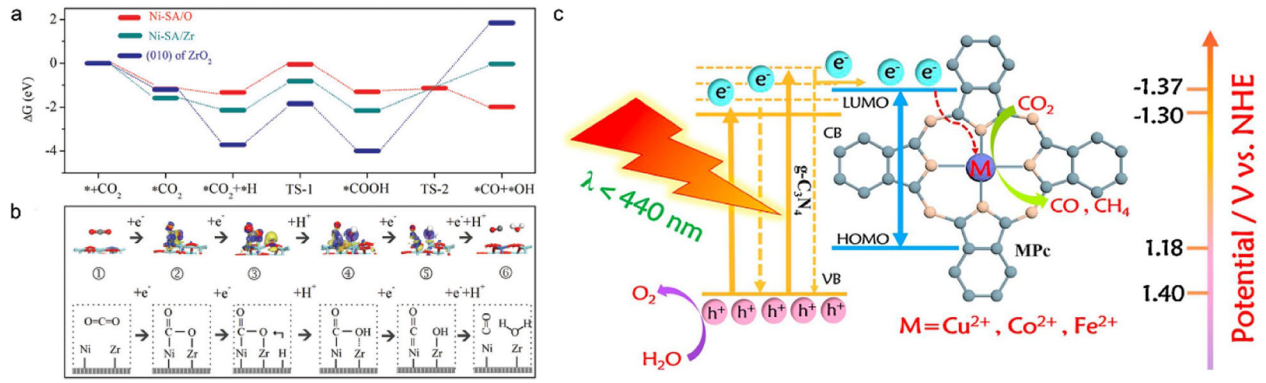

Fig. 5 (**a**) Energy profile for the elementary steps of CO_2 reduction to CO over (010) facets of ZrO_2, Ni-SA/Zr, and Ni-SA/O (**b**) Differential charge density diagrams and intermediates during CO_2 reduction to CO over Ni-SA/O model [23] Copyright 2020, Wiley-VCH (**c**) Schematic of HLEEs transfer process in the fabricated MPc/CN heterojunction [24] Copyright 2020, Elsevier

transient absorption spectroscopy (TAS), which is a powerful technique to directly reveal the charge carrier dynamics of photocatalysts. The half-life time of the signal observed at 700 nm of CN increased from 25 μs to 160 μs after decorating with ^{m}CD, indicating suppressed electron-hole recombination owing to the charge separation across the ^{m}CD/CN junction (Fig. 6). Accordingly, it offers longer time for the 6-electron process to reduce CO_2 to methanol.

Based on the discovery that carbon-dots could act as a hole acceptor of CN, Tang and Godin et al. further modulated the fine structure of CN from the perspective of band positions, bandgaps and hydrophilicity to stepwise optimize the photocatalytic activity of CN, and followed by modification of CD with the function of extracting holes [26]. A carbon nitride-like polymer (FAT) was designed by altering the terminal and linker groups in carbon nitride, and the replacement of some N atoms in CN to O atoms in FAT leading to a higher intensity of trapped holes with photoexcitation, which is different from the common CN with the nature of trapping electrons. As expected, the CD decorated FAT manifested impressive activity for selective CO_2 reduction to methanol by water. It was evidenced by TAS that the fast hole trapping in FAT is the key because of the CD can subsequently capture holes on the sub-microsecond timescale. This work proposed a significant thought to improve the activity from the perspective of retaining the reactivity of holes and increase the number of effective electrons, so as to accelerate the six-electron reduction of CO_2 conversion to methanol.

As stated before, modulating the photogenerated holes to facilitate water oxidation is a crucial aspect which needs to be considered in the course of CO_2 photoreduction. It is naturally expected that regulating the photogenerated electrons on the foundation of hole trapping is bound to build a fancy photocatalytic system with high performance for CO_2 reduction. Jing et al. developed a facile and green approach to anchor subnano Ni and Mn-oxo clusters on chitosan oligomer (COS)-functionalized ultrathin g-C_3N_4 (UCN) nanosheet for efficient CO_2 conversion [27]. The decorated Ni-oxo and Mn-oxo clusters with an average diameter of ca. 0.8 nm were supported on $5COS_{20}$–UCN uniformly (Fig. 7a-c). Atmosphere-controlled SPS spectra uncovered the character of Ni-oxo clusters for capturing electrons, since the SPS response of 1.5Ni–$5COS_{20}$–UCN in O_2 is stronger compared with that in N_2 with the generally acknowledged O_2 capture electrons. While Mn-oxo clusters decorated $5COS_{20}$-UCN delivered an opposite result, and the SPS signals of 1Mn–$5COS_{20}$–UCN in O_2 are weaker than that in N_2 atmosphere, which is indictive of the nature of Mn-oxo clusters for capturing holes (Fig. 7d). These results are further confirmed by TS-SPV spectra in N_2 atmosphere. Interestingly, the response of the optimal 1Ni0.75Mn–$5COS_{20}$–UCN shows a less-positive response than 1.5Ni–$5COS_{20}$–UCN, which strongly evidenced the dual modulation of photogenerated electrons and holes by Ni and Mn-oxo clusters (Fig. 7e). Moreover, collaborated with the results of electrochemical measurements, the synergetic effect between Ni- and Mn-oxo species, is capable of photogenerated electron trapping along with CO_2 activation and photogenerated hole trapping along with water activation are clarified (Fig. 7f and g). Matching capacity of Ni- and Mo-oxo species for the equalized modulation of electrons and holes is highlighted for the first time.

Likewise, they fabricated MnO_x and Au-TiO_2 co-modified porous g-C_3N_4 as efficient visible light responsive photocatalysts for CO_2 reduction. The lifetime of photogenerated charge carriers of g-C_3N_4 is greatly prolonged with the decoration of sheet-like nanostructured

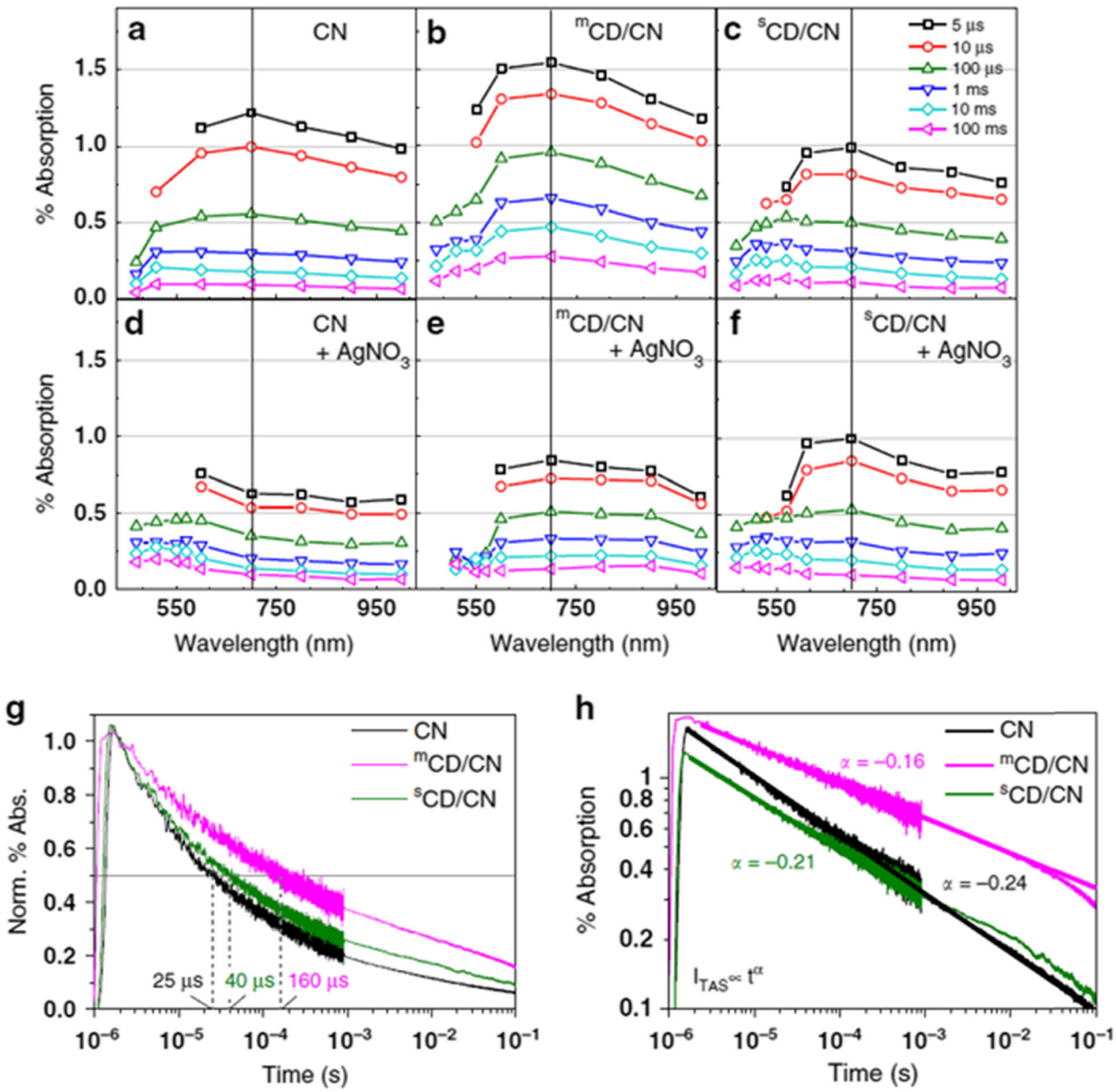

Fig. 6 Diffuse reflectance TAS spectra for samples with (**a**–**c**) and without (**d**–**f**) 10 mM $AgNO_3$ (**g**) µs-TAS decay kinetics of CN, ^{m}CD/CN and ^{s}CD/CN in water monitored at 700 nm and excited by pulsed 355 nm excitation (460 µJ/cm^2) and (**h**) fitted α parameters indicated in the same color as the associated trace [20] Copyright 2020, Springer Nature

MnO_x, which is disclosed by transient-state surface photovoltage (TS-SPV) response, an advanced technique to investigate the dynamic properties of charge carriers. It is deduced that the modified MnO_x could capture holes and afford catalytic function for H_2O oxidation for producing hydroxyl and then evolving oxygen, while the coupled Au on TiO_2 could trap electrons and provide catalytic active sites for CO_2 reduction. Accordingly, the optimal one delivers impressive CO_2 conversion activity and quantum efficiency of ≈4.92% at 420 nm wavelength [28].

4.3 Promoting charge separation by constructing Z-scheme heterojunctions

As stated above, modification of cocatalyst on a single photocatalyst whose CB and VB could meet the thermodynamic potentials for both CO_2 reduction and water oxidation, is an effective strategy to accelerate the surface reaction kinetics, and simultaneously enhance the charge separation. However, it often requires a semiconductor endowed with a wide bandgap. In contrast, narrow bandgap semiconductors are helpful due to the

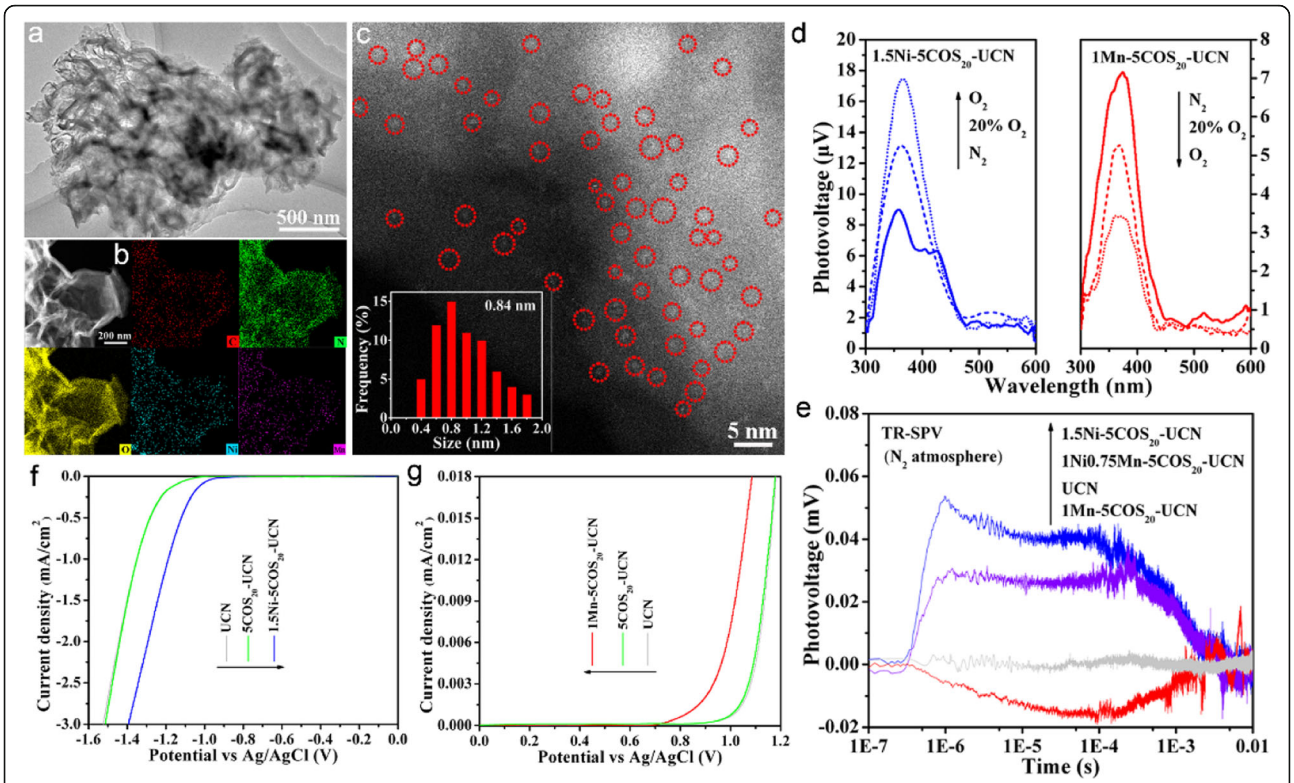

Fig. 7 (**a**) TEM image, (**b**) STEM image and the corresponding EDX mapping images of C, N, O, Ni, and Mn elements, and (**c**) HAADF-STEM image of 1Ni0.75Mn–COS_{20}–UCN (**d**) SPS responses of 1.5Ni–COS_{20}–UCN (left) and 1Mn–COS20–UCN (right) in different atmospheres (**e**) TS-SPV responses of UCN, 1Mn–COS_{20}–UCN, 1.5Ni–COS_{20}–UCN, and 1Ni0.75Mn–$5COS_{20}$ UCN in the N_2 atmosphere (**f**) EC reduction curves of UCN, $5COS_{20}$–UCN and 1.5Ni–COS_{20}–UCN in the CO_2-bubbled system (**g**) EC oxidation curves of UCN, $5COS_{20}$–UCN and 1Mn–COS_{20}–UCN samples in the N_2-bubbled system [27] Copyright 2021, Wiley-VCH

wide visible light absorption range. Whereas, in most cases, it suffers from the insufficient reduction capacity of electrons or inadequate oxidation capacity of holes. Unfortunately, these two aspects are contradictory and, in consequence, the concept of heterojunction emerges on the scene.

Several types of heterojunctions have been explored in recent decades, in which the traditional type II heterojunction has been widely investigated and received considerable attention [15, 17, 77]. In fact, the type II heterojunction could suppress the recombination of charge carriers, while the charge separation is promoted by sacrificing the strong redox capacities of those photogenerated charge carriers, which is detrimental to CO_2 conversion with high thermodynamic requirements. Hence, developing a heterojunction with rapid charge separation and meanwhile maintaining the sufficient thermodynamic energy of photoelectrons and holes, is anticipated to be a more rational option to improve the photocatalytic activities for CO_2 reduction.

Enlightened by nature photosynthesis, constructing artificial Z(S)-scheme heterojunction via linking two semiconductors with staggered band structures has emerged as a fancy pathway to convert CO_2 with water into solar fuels. On one hand, the charge separation would be greatly facilitated with the help of recombination of the charge carriers with weak redox capacities. On the other hand, what makes it distinct from type II heterojunctions lie in the energetic electrons of the reductive semiconductor and the positive holes of the oxidative semiconductor could be preserved, which provides sufficient energy to drive the overall CO_2 reduction reaction. In this regard, it is feasible to construct a Z(S)-scheme heterojunction by combining a CO_2 reduction photocatalyst and a water oxidation photocatalyst for efficient CO_2 conversion.

Zhou et al. fabricated a high-performance $BiVO_4${010}–Au–Cu_2O Z-scheme photocatalyst for CO_2 reduction from the view of charge separation [18]. This research pointed out that the hot electrons that accumulate on the {010} surface of $BiVO_4$ could easily overcome the Schottky barrier to facilitate the migration from $BiVO_4$ to Au, and then recombine with the photogenerated holes in Cu_2O. The long-live holes and electrons in the VB of $BiVO_4$ and CB of Cu_2O due to the deposition of crystal-facet-dependent

electron shuttle could initiate water oxidation to produce O_2 and CO_2 reduction to CO and CH_4 with high-efficiency, respectively (Fig. 8a). This study integrated surface-induced charge directional transfer and the optimal contact interface, and provided a new strategy for designing efficient Z-scheme heterojunction for CO_2 reduction. Similarly, a three-dimensional $BiVO_4$/Carbon-Coated Cu_2O nanowire arrays were synthesized for CO_2 conversion to CO and CH_4 (Fig. 8b) [78]. The charge separation is significantly enhanced due to the construction of Z-scheme heterojunction, and as a result, the CO formation rate over BVO/C/Cu_2O exhibited ca. 9- and 5-fold improvements than those of Cu_2O mesh and Cu_2O NWAs, respectively (Fig. 8c). The accelerated Z-scheme charge flow between BVO and Cu_2O with the introduced carbon layer plays a crucial role in improving the photocatalytic activities. In addition, the BVO/C/Cu_2O heterojunction delivered outstanding stability in the course of CO_2 photoreduction with the help of incorporation of a carbon protective layer.

It is worth noting that the current Z-scheme systems for CO_2 reduction still remains a great challenge on account of the inefficient interfacial charge transfer along with the competitive side and back reactions, namely the proton reduction and the oxidation of the reduction products from CO_2 conversion. In this condition, it is difficult to control the selectively of the CO_2 reduction products, in particular associated with the use of redox mediators. Demon and Reisner et al. innovatively proposed a photocatalyst sheet that converts CO_2 and H_2O into formate and oxygen as a potentially scalable technology for CO_2 utilization [29]. La- and Rh-doped $SrTiO_3$ ($SrTiO_3$:La,Rh) and Mo-doped $BiVO_4$ ($BiVO_4$:Mo) were integrated on to a gold layer as the CO_2 reduction and water oxidation photocatalysts, respectively. Meanwhile, phosphonated Co(II) bis(terpyridine) and RuO_2 were loaded on the reductive photocatalyst and the oxidative counterpart. The Z-scheme charge which transfers between $BiVO_4$:Mo and $SrTiO_3$:La,Rh is greatly facilitated with the modification of Au layer, and the modified CotpyP and RuO_2 were evidenced as highly

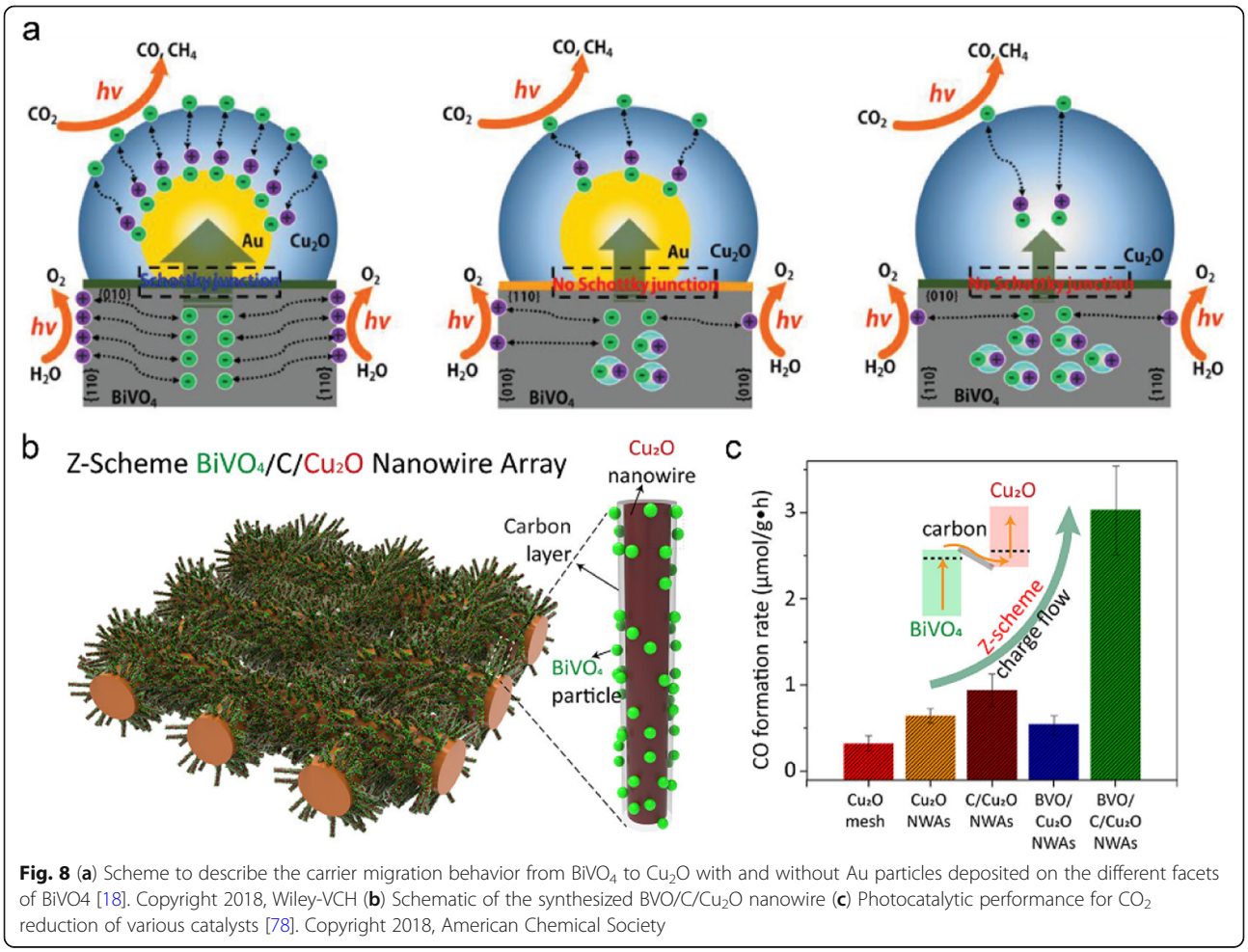

Fig. 8 (**a**) Scheme to describe the carrier migration behavior from $BiVO_4$ to Cu_2O with and without Au particles deposited on the different facets of BiVO4 [18]. Copyright 2018, Wiley-VCH (**b**) Schematic of the synthesized BVO/C/Cu_2O nanowire (**c**) Photocatalytic performance for CO_2 reduction of various catalysts [78]. Copyright 2018, American Chemical Society

efficient cocatalysts for CO_2 reduction and oxygen evolution, respectively. The enhanced charge separation and the accelerating surface reaction kinetics contribute to the excellent CO_2 reduction performance. The well-designed monolithic device delivered a superior solar-to-formate conversion efficiency of 0.08 ± 0.01% with a selectivity for formate of 97 ± 3%. The apparent quantum yield (AQY) at 420 ± 15 nm was achieved to 2.6%. Moreover, the produced $HCOO^-$ with an STF of 0.06% was obtained on a sheet with an active irradiated area of ca. 20 cm^2. This impressive wireless device combines formate production and water oxidation with light as the sole energy source, which has seldom been reported in the field of wireless CO_2 reduction.

Modifying cocatalysts on Z-scheme heterojunctions has been evidenced as a feasible strategy to lower the barrier of CO_2 activation and improve the selectivity, yet the capacity of cocatalysts for the manipulation of Z-scheme charge separation still limited. While the rapid charge separation is the prerequisite for the subsequent CO_2 concentration and surface catalytic reactions. To this end, to further modulate the Z-scheme charge transfer and separation are crucial to boost the photocatalytic activities of CO_2 reduction. On one hand, the charge transfer and migration of both reductive and oxidative semiconductor along with the successful interfacial transfer influence the Z-scheme performance. On the other hand, the competitive type II charge transfer pathway (electrons transfer from the reductive seminconductor to the oxidative one, while the holes transfer in the opposite direction) due to the staggered band structures of the reductive photocatalyst and the oxidative photocatalyst would severely impair the Z-scheme charge transfer and separation. Accordingly, tackling the issues of interfacial charge transfer and modulating the desirable Z-scheme charge transfer pathway are of great significance for the architecture of highly efficient Z-scheme heterojunction.

Very recently, Jing and Tang et al. proposed a universal strategy to construct a cascade Z-scheme system with dimension-matched (001)TiO_2-g-C_3N_4/$BiVO_4$ nanosheet (T-CN/BVNS) heterojunction as a model [30]. The coupled (001)TiO_2 serving as an effective energy platform could direct Z-scheme charge transfer and separation, blocking the unexpected type-II charge transfer pathway (Fig. 9a). The optimal T-CN/BVNS heterojunction exhibits ca.19-fold photoactivity improvement for CO_2 reduction to CO in the absence of cocatalysts and costly sacrificial agents under visible-light irradiation, compared with pristine $BiVO_4$ nanosheet, which is also superior to other reported Z-Scheme systems even with noble metals as mediators. Notably, the introduced (001)TiO_2 could prolong the lifetimes of spatially separated electrons and holes and does not compromise their reduction and oxidation potentials, which was comprehensively validated by experimental results and DFT calculations from the view of ultrafast timescale. Importantly, this strategy is also applicable to facilitate the charge transfer in other Z-scheme heterojunctions (eg.C_3N_4/WO_3 and C_3N_4/Fe_2O_3), and other wide-band gap semiconductors, such as SnO_2, can also be used as an alternative electron-energy platform. Overall, this study highlights photocatalysts with advanced charge separation property is vital to achieve CO_2 photoreduction activity improvement, and enrich the methods for the design of delicate Z-scheme heterojunction with cascade charge transfer.

In another study, Li et al. reported a Cu_2O–Pt/SiC/IrO_x hybrid photocatalyst by loading the IrO_x and Pt-Cu_2O on SiC surface through a step-by-step photodeposition method, and integrated with Pt/WO_3 to construct an artificial photosynthetic system [31]. Interestingly, a spatially separated reaction system with two reaction chambers was established, in which one chamber is loaded with the Cu_2O–Pt/SiC/IrO_x hybrid and Fe^{2+} for CO_2 reduction, and the other one with Pt/WO_3 and Fe^{3+} for water oxidation (Fig. 9b and c). Benefitting from the elaborately design, the artificial photosynthetic system exhibits superior photocatalytic activities for CO_2 reduction to HCOOH and H_2O oxidation to O_2 under visible light irradiation. Importantly, the yields of HCOOH and O_2 with stoichiometric ratio achieved 896.7 and 440.7 μmol g^{-1} h^{-1}, respectively. It is revealed that the impressive efficiencies of CO_2 conversion and water oxidation are ascribed to the unique configuration of direct Z-scheme electronic structure of Cu_2O-Pt/SiC/IrO_x and the indirect Z-scheme spatially separated reduction and oxidation units, which enables photogenerated electrons and holes live longer and hold back the backward reaction of products.

Enormous studies about photocatalyst have been conducted by integrating the water oxidation with a CO_2 reduction to construct Z-scheme heterojunctions for CO_2 reduction by pure water [32, 54, 55, 57]. In addition to the traditional Z-scheme heterojunction with typical inorganic semiconductors as reductive constituents, some organic materials are emerged as a new frontier on account of the potentials for CO_2 adsorption, diffusion and activation. Recently, crystalline covalent organic frameworks (COFs) have attracted great attention and been continually developed. In particular, the rich porous structure and the tunable energy band alignments make it a desirable reductive photocatalyst for the construction of a novel Z-scheme heterojunction.

Lan et al. developed a versatile strategy to fabricate series of COF-semiconductor Z-scheme heterojunctions for CO_2 conversion, in which the water oxidation photocatalysts (TiO_2, Bi_2WO_6, Fe_2O_3) were elaborately integrated with COFs (COF-316/318) by covalent

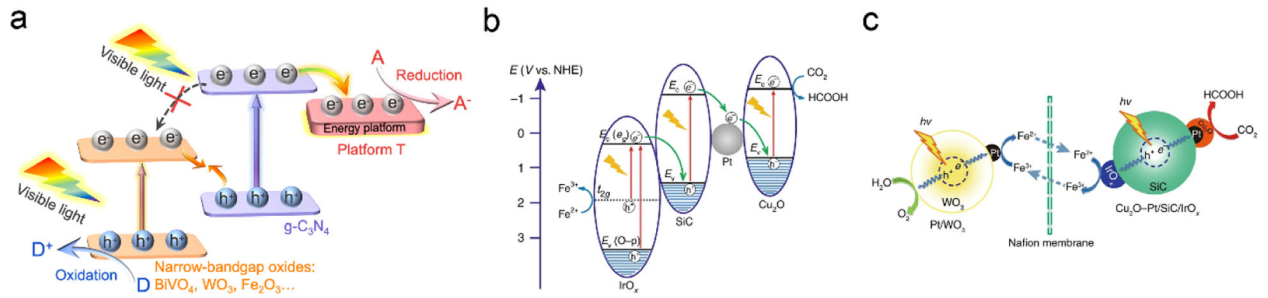

Fig. 9 (**a**) Schematic representation of the proposed cascade Z-Scheme mechanism of photogenerated charge transfer under visible light for efficient photocatalysis. T refers to (001)TiO_2, which can feasibly be replaced by other wide bandgap semiconductors like SnO_2 [30] Copyright 2021, Wiley-VCH (**b**) The electron transfer processes in Cu_2O–Pt/SiC/IrO_x under light illumination (**c**) The proposed mechanism of the separated system for the efficient CO_2 reduction and O_2 evolution [31] Copyright 2020, Springer Nature

connection [32]. The optimal COF-318-TiO_2 Z-scheme heterojunction delivered the highest CO production rate of 69.67 μmol/g/h in the absence of additional photosensitizers and sacrificial agents, 5.2-fold and 6-time higher than the pure COF-318 and TiO_2, respectively (Fig. 10a and b). Meanwhile, the produced O_2 has also been confirmed by the isotope labeling experiment. Both experimental results and DFT calculations revealed the Z-scheme charge transfer pathway in the COF-semiconductor heterojunctions, resulting in the spatial separated electrons accumulated in COF for CO_2 reduction and the photogenerated holes leave in semiconductors for water oxidation. It also pointed out that the energy barrier for CO_2 activation is reduced due to the coexistence of pyridine group and cyano sites (Fig. 10c and d). The inherent CO_2 uptake capacity of COFs makes it different from traditional reductive photocatalyst. This study is the first case of COF-semiconductor Z-scheme heterojunction in the application of CO_2 reduction by pure water, and it can be seen that the efficient charge transfer and separation are of significance as well as in the organic-inorganic Z-scheme heterojunction towards CO_2 reduction.

In the latest decade, the concept of isolated active site has been a hot topic in fields of photocatalysis and electrocatalysis. The isolated active site could maximize metal atom utilization efficiency and provide abundant active centers for the targeting reactions. Integrating the merits of Z-scheme dominant rapid charge separation and isolated active sites for CO_2 activation would undoubtedly improve the photocatalytic activities for CO_2 reduction. Jing and co-workers innovatively developed a zinc phthalocyanine/$BiVO_4$ nanosheet (ZnPc/BVNS) ultrathin nanocomposites for CO_2 photoreduction via a

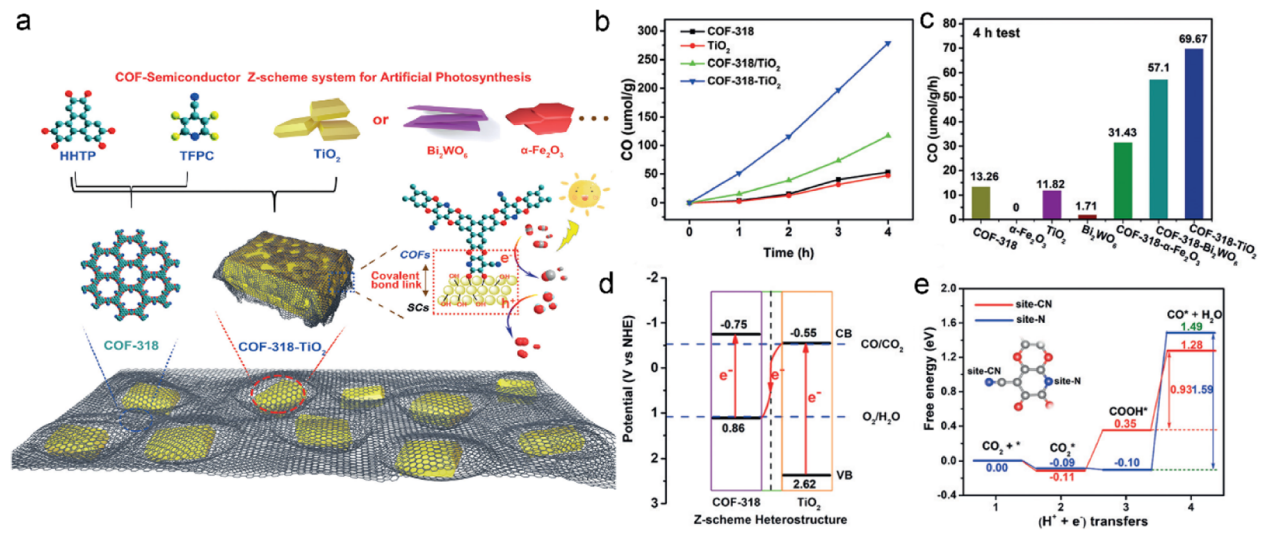

Fig. 10 (**a**) Schematic representation of the preparation of COF-318-SCs via the condensation of COF-318 and semiconductor (**b**) Photocatalytic CO_2 to CO performances of COF-318-TiO_2 for gas-solid CO_2 reduction compared with COF-318, TiO_2 and COF-318/TiO_2 (**c**) Photocatalytic performances of various COF-318-SCs and bulk COF-318, TiO_2, Bi_2WO_6 and α-Fe_2O_3 (**d**) Schematic illustration of the charge transfer process under light irradiation with Z-scheme model (**e**) CO_2 RR process on COF-318-TiO_2 based on DFT calculations [32] Copyright 2020, Wiley-VCH

hydroxyl induced assembly strategy (Fig. 11a) [33]. The optimal one delivers ca. 16-fold enhancement in the quantum efficiency compared with the reported $BiVO_4$ nanoparticles at the excitation of 520 nm with an assistance of 660 nm photons. In addition, a certain amount of oxidation product O_2 with stoichiometric ratio is also produced. The impressive activities are primarily attributed to the cascade Z-scheme charge transfer between ZnPc and BVNS thanks to the dimension-matched ultrathin heterojunction nanostructure, which is comprehensively validated by experimental results and theoretical calculations (Fig. 11b-d). Importantly, the spatial separated electrons could be further transferred from the ligand of ZnPc to the isolated Zn-N_4 catalytic sites, leading to the accelerated CO_2 adsorption and activation (Fig. 11e). This work proposed a delicate reductive photocatalyst ZnPc which is distinguished from traditional ones, featuring isolated catalytic active sites and wide visible light absorption properties. This novel Z-scheme heterojunction opens up a new route for the design of highly efficient photocatalysts for CO_2 reduction from the perspective of both charge separation and catalytic active sites introduction.

Since the pioneering work of the new step-scheme (S-scheme) heterojunction with WO_3/g-C_3N_4 as the first model was reported in 2019, plenty of related research is undergoing rapid development [79]. The emergence of S-scheme heterojunctions is based on the direct Z-scheme heterojunctions, while it aims to reveal the photocatalytic mechanism clearly and vividly. The charge transfer route in the S-scheme heterojunction is similar to the Z-scheme one, that is, the photogenerated electrons in the CB of oxidation photocatalyst would recombine with the photogenerated holes in the VB of reduction photocatalyst, and the spatial separated electrons and holes with high reductive and oxidative capacities could be preserved to initiate redox reactions. While the recombination step of the pointless electrons and holes in S-scheme heterojunctions is emphasized with the driving force, namely, the internal electric field, band bending, and Coulombic attraction. In this condition, the S-scheme heterojunction dominant charge separation would be more powerful than Z-scheme ones.

Yu et al. fabricated a unique 2D van der Waals heterostructure of Ti_3C_2 MXene quantum dots decorated TiO_2/C_3N_4 nanosheets for CO_2 photoreduction into hydrocarbon fuels [34]. The constructed 2D/2D/0D $TiO_2/C_3N_4/Ti_3C_2$ heterojunction exhibits much higher photocatalytic CO_2 reduction activity compared with that of TiO_2, C_3N_4, TiO_2/C_3N_4 and C_3N_4/Ti_3C_2. The S-scheme heterojunction at the TiO_2/C_3N_4 interface plays a critical role in enhancing the charge separation, and the formation of Schottky heterojunction at the C_3N_4/Ti_3C_2 quantum dots interface further facilitate the electrons transfer from C_3N_4 to Ti_3C_2 quantum dots. This charge modulation strategy is similar with the above

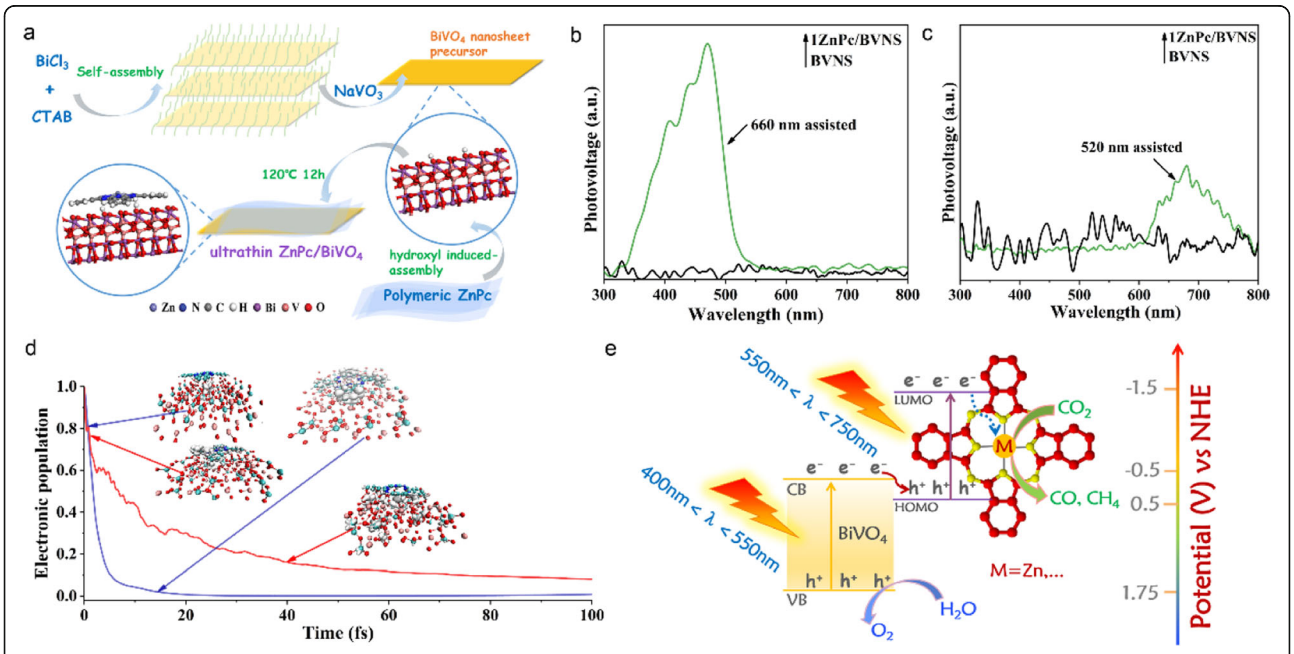

Fig. 11 (**a**) Schematic illustration of the preparation of ultrathin ZnPc/BVNS heterojunction. SPS responses of 1ZnPc/BVNS and BVNS in N_2 atmosphere assisted with a (**b**) 660 nm and (**c**) 520 nm monochromatic beam (**d**) The time-dependent survival probability (TDSP) curves of the excited electrons transfer between partly hydroxylated BVNS and ZnPc during the injection process (Red: from ZnPc to BVNS; Blue: from BVNS to ZnPc) (**e**) Proposed cascade Z-scheme mechanism of photogenerated charge transfer on MPc-coupled BVNS. M represents a transition metal [33] Copyright 2019, Wiley-VCH

mentioned one (T-CN/BVNS), in which TiO_2 as the energy platform to direct charge transfer in the cascade Z-scheme heterojunction [30]. It can be concluded that to maximized the charge transfer and separation is vital to the improvement for the photocatalytic activities for CO_2 reduction.

5 Conclusions and perspectives

At present, some significant advances in photocatalytic CO_2 reduction have been achieved, especially on the strategies for improving the activities of CO_2 photoreduction which concentrated on the CO_2 adsorption and activation, water oxidation kinetics acceleration, and highly efficient charge transfer and separation. Even though some successes have been made in designing CO_2 reduction systems, and reveal the reaction mechanism and pathway, the desirable activity and the selectivity of the target products are still in their infancy stage. There are still several perspectives for improvement in further architecture of photocatalysts toward solar fuels production with great challenges ahead.

First of all, comprehensive photocatalytic CO_2 reduction systems with strong light absorption capacity, rapid charge separation property, and abundant catalytic active sites need to be developed. It is well acknowledged that the overall efficiency of CO_2 reduction depends on these three core parameters, while the selectivity is determined by both the thermodynamic potential and kinetic energy barriers in terms of the CO_2 reduction pathway. Heterojunction photocatalysts, especially for Z(S)-scheme ones could tackle the irreconcilable aspects of visible light harvesting and the large bandgap as far as the sufficient redox potentials. Hence, rational design oxidative and reductive constituents with emerging materials, such as COFs, MOFs, and functional metal phthalocyanines, etc. that endowed with broad visible light response and catalytic active sites to construct integrative Z(S)-scheme heterojunctions, are promising routes to access the desirable photocatalytic CO_2 performance. Importantly, the tunable energy band alignments, enriched porous structure, the well-defined coordination environment and the isolated active sites provide plenty of opportunities for rationalizing the configuration of Z(S)-scheme heterojunctions, as well as improving the selectivity for the target reduction products.

An additional challenge is the standardized evaluation of the CO_2 photoreduction performance. Most current studies quantified the photocatalytic activities of CO_2 reduction via the formation rate of a certain product, and the final performance is presented in terms of μmol h^{-1}, or μmol $h^{-1} g^{-1}$ by normalizing the mass of the used photocatalyst. However, it is not quite rational for the comparison between different works in this way since the varieties of reaction systems, light intensities, and the mass of the used photocatalyst, etc. Even though to quantify the photocatalytic activities of CO_2 reduction by AQY could improve the accuracy of the performance evaluation, it is still somewhat not accurate as one hole scavenger can dramatically affect AQY. Therefore, a specific and unified regulation is essential to be established, including light source (wavelength and intensity), irradiation areas, photocatalyst dosage, and the volume of the used water, etc. Alternatively, the solar-to-chemical conversion efficiency which reflects the energy conversion ability of a photocatalyst could also be determined as a key criterion to evaluate the performance of CO_2 photoreduction.

A critical issue that should be taken into account in CO_2 photoreduction is the modulation of water oxidation half-reaction. It is accepted that the water oxidation half-reaction is a more challenging and rate-determining step in the overall CO_2 reduction reactions. Whereas, very few studies are focused on the oxidative aspect. The typical modulation strategies for facilitate O_2-evolution in photocatalytic water splitting are also applicable in designing the oxidative constituents of heterojunctions towards efficient CO_2 reduction and water oxidation.

Adjusting the selectivity of product is of great significance to improve the yield of high-value-added chemicals or even liquid fuels. Generally, water is more preferentially adsorbed onto the surface of photocatalysts than CO_2. Undoubtedly, the fierce competing HER is inevasible in CO_2 photoreduction by water. On one hand, it is feasible to introduce precise active sites such as metal single atoms with highly selective adsorption ability toward CO_2 molecules in order to guarantee the CO_2 instead of water to be reduced first. On the other hand, to achieve C=O bond cleavage and C-H bond formation simultaneously is imperative. Construction of ingenious dual sites with different functions of C=O bonds activation and hydrogenation is a viable strategy to access CO_2 conversion to CH_4. The d-band centers and the geometric structures for transition-metal atoms would be easily influenced when combining with another metal, and the electronic structure change could favor the sustainable multi-electron attracted CO_2 reduction process to hydrocarbon. Another crucial direction for improving the selectivity of CO_2 photoreduction lies in the rational design of photocatalysts. Considering the inherent characters of the employed photocatalyst for CO_2 adsorption, porous materials such as zeolites and metal-organic frameworks (MOFs), etc. with high surface areas, tunable porous structures, pore volumes, and dimensionalities are promising candidates to capture CO_2 molecules in their cavities for selective CO_2 conversion. The confinement of pores would play vital role in restricting reaction intermediates to achieve hydrogenation for the CH_4 production. Beyond that, the surface

modification of photocatalysts would governing the CO_2 adsorption, activation, and further the selectivity. For instance, the engineering of surface defects includes oxygen vacancies, sulfur vacancies, the introduction of functional Lewis basic sites, as well as loading targeted noble-metal cocatalysts. Moreover, it is challenging convert CO_2 to multicarbon fuels with high energy density. The key step for the transformation of CO_2 to C_{2+} products is the sluggish kinetics process of C-C coupling. To stabilize and enrich the related intermediates on the active sites of a photocatalyst would allow the intermediates to be further protonated as well as increase the C-C coupling possibility, resulting in the evolution of C_{2+} or liquid products.

Another vital aspects are the identification of the active sites in CO_2 conversion, revelation of the mechanism of reaction process, and reaction pathway, which are favorable for the understanding of product selectivity of CO_2 reduction. In general, the identification of active sites could be achieved only under reacting conditions. Therefore, to precisely and comprehensively confirm the active sites with advanced characterization techniques is always pursued, especially in-situ and time resolved ones. For instance, in-situ Raman spectroscopy could deliver detailed information about chemical structures, and investigate the interactions between active sites of the photocatalyst and the adsorbed reactant. In situ nearly ambient pressure XPS (NAP-XPS) under working conditions is a powerful technique to reveal the intermediates species on the catalyst during the process of photocatalysis. Combining with the information of the detected change of surface groups and intermediates on a photocatalyst by in-situ Fourier transform infrared spectroscopy (FT-IR), a convincible and comprehensive process of CO_2 conversion on active sites could be deduced. Meanwhile, the acquired information about reaction process kinetics and possible intermediate radicals could also reveal the selectivity of products. In addition, in situ electron paramagnetic resonance (EPR) spectroscopy could detect the unpaired electrons or radicals, which normally formed on the active sites. In this regard, the involved charge transfer associated with active sites in CO_2 conversion could be directly unveiled by in-situ EPR measurement. Moreover, TAS is a powerful tool to uncover the electron-hole dynamics of semiconductors at a wide timescale. Although the applications of TAS in the field of CO_2 reduction are still limited, the development of in-situ and operando TAS with specific conditions (different atmosphere along with the saturated aqueous solution) would deeply elucidate the complicated reaction process of CO_2 reduction by pure water from the perspective of charge carrier dynamics.

Abbreviations

CO_2: carbon dioxide; TEOA: triethanolamine; TEA: trimethylamine; EDTA: ethylenediaminetetraacetic acid; MOF: metal-organic framework; HER: hydrogen evolution reaction; VB: valence band; CB: conduction band; LUMO: lowest unoccupied molecular orbital; TCD: thermal conductivity detector; FID: flame ionization detector; MPc: metal phthalocyanine; ^{m}CD/CN: carbon-dots decorated carbon nitride; TAS: transient absorption spectroscopy; FAT: carbon nitride-like polymer; COS: chitosan oligomer; UCN: ultrathin g-C_3N_4; TS-SPV: transient-state surface photovoltage; $SrTiO_3$:La,Rh: La- and Rh-doped $SrTiO_3$; $BiVO_4$:Mo: Mo-doped $BiVO_4$; AQY: apparent quantum yield; T-CN/BVNS: (001)TiO_2-g-C_3N_4/$BiVO_4$ nanosheet; COFs: covalent organic frameworks; ZnPc/BVNS: zinc phthalocyanine/$BiVO_4$ nanosheet; S-scheme: step-scheme; FT-IR: Fourier transform infrared spectroscopy

Acknowledgements

JB, ZZ, YL and LJ are thankful for the financial support by the National Natural Science Foundation of China (no. U1805255, U2102211). EC and JT thank the financial support from the Royal Society Newton Advanced Fellowship grant (NAF\R1\191163), UK EPSRC (EP/S018204/2), Leverhulme Trust (RPG-2017-122), and Royal Society Leverhulme Trust Senior Research Fellowship (SRF\R1\21000153).

Authors' contributions

JB and ZZ drafted the manuscript. YL helped to collect the literatures. EC concentrated on discussion and language. JT and LJ conceived of the review and revised the manuscript. All authors read and approved the final manuscript.

Funding

National Natural Science Foundation of China (no. U1805255, U2102211), Royal Society Newton Advanced Fellowship grant (NAF\R1\191163), UK EPSRC (EP/S018204/2), Leverhulme Trust (RPG-2017-122) and Royal Society Leverhulme Trust Senior Research Fellowship (SRF\R1\21000153).

Availability of data and materials

Not applicable.

Declarations

Ethics approval and consent to participate

Not applicable.

Consent for publication

Not applicable.

Competing interests

The authors declare no competing financial interest.

Received: 18 November 2021 Accepted: 24 January 2022
Published online: 19 April 2022

References

1. Zickfeld K, Azevedo D, Mathesius S, Matthews HD (2021) Asymmetry in the climate-carbon cycle response to positive and negative CO_2 emissions. Nat Clim Chang 11(7):613–617. https://doi.org/10.1038/s41558-021-01061-2
2. Bonnet R, Swingedouw D, Gastineau G, Boucher O, Deshayes J, Hourdin F, Mignot J, Servonnat J, Sima A (2021) Increased risk of near term global warming due to a recent AMOC weakening. Nat Commun 12(1):6108. https://doi.org/10.1038/s41467-021-26370-0
3. Voiry D, Shin HS, Loh KP, Chhowalla M (2018) Low-dimensional catalysts for hydrogen evolution and CO_2 reduction. Nat Rev Chem 2(1):0105. https://doi.org/10.1038/s41570-017-0105
4. Blankenship RE, Tiede DM, Barber J, Brudvig GW, Fleming G, Ghirardi M, Gunner MR, Junge W, Kramer DM, Melis A, Moore TA, Moser CC, Nocera DG, Nozik AJ, Ort DR, Parson WW, Prince RC, Sayre RT (2011) Comparing photosynthetic and photovoltaic efficiencies and recognizing the potential for improvement. Science 332(6031):805–809. https://doi.org/10.1126/science.1200165

5. Jiao XC, Zheng K, Hu ZX, Sun YF, Xie Y (2020) Broad-spectral-response photocatalysts for CO_2 reduction. ACS Cent Sci 6(5):653–660. https://doi.org/10.1021/acscentsci.0c00325
6. Li X, Yu JG, Jaroniec M, Chen XB (2019a) Cocatalysts for selective photoreduction of CO_2 into solar fuels. Chem Rev 119(6):3962–4179. https://doi.org/10.1021/acs.chemrev.8b00400
7. Li A, Wang T, Li CC, Huang ZQ, Luo ZB, Gong JL (2019b) Adjusting the reduction potential of electrons by quantum confinement for selective photoreduction of CO_2 to methanol. Angew Chem Int Ed 58(12):3804–3808. https://doi.org/10.1002/anie.201812773
8. Bie CB, Zhu BC, Xu FY, Zhang LY, Yu JG (2019) In situ grown monolayer N-doped graphene on Cds hollow spheres with seamless contact for photocatalytic CO_2 reduction. Adv Mater 31(42):1902868. https://doi.org/10.1002/adma.201902868
9. Wu JH, Huang Y, Ye W, Li YG (2017a) CO_2 reduction: from the electrochemical to photochemical approach. Adv Sci 4(11):1700194. https://doi.org/10.1002/advs.201700194
10. Inoue T, Fujishima A, Konishi S, Honda K (1979) Photoelectrocatalytic reduction of carbon dioxide in aqueous suspensions of semiconductor powders. Nature 277(5698):637–638. https://doi.org/10.1038/277637a0
11. Sun ZY, Talreja N, Tao HC, Texter J, Muhler M, Strunk J, Chen J (2018) Catalysis of carbon dioxide photoreduction on nanosheets: fundamentals and challenges. Angew Chem Int Ed 57(26):7610–7627. https://doi.org/10.1002/anie.201710509
12. Xu YF, Yang MZ, Chen BX, Wang XD, Chen HY, Kuang DB, Su CY (2017) A $CsPbBr_3$ perovskite quantum dot/graphene oxide composite for photocatalytic CO_2 reduction. J Am Chem Soc 139(16):5660–5663. https://doi.org/10.1021/jacs.7b00489
13. Sheng H, Oh MH, Osowiecki WT, Kim W, Alivisatos AP, Frei H (2018) Carbon dioxide dimer radical anion as surface intermediate of photoinduced CO_2 reduction at aqueous cu and cdse nanoparticle catalysts by rapid-scan FT-IR spectroscopy. J Am Chem Soc 140(12):4363–4371. https://doi.org/10.1021/jacs.8b00271
14. Fu YH, Sun DR, Chen YJ, Huang R, Ding Z, Fu X, Li Z (2012) An amine-functionalized titanium metal-organic framework photocatalyst with visible-light-induced activity for CO_2 reduction. Angew Chem Int Ed 51(14):3364–3367. https://doi.org/10.1002/anie.201108357
15. Wang DK, Huang RK, Liu WJ, Sun DR, Li ZH (2014a) Fe-based mofs for photocatalytic CO_2 reduction: role of coordination unsaturated sites and dual excitation pathways. ACS Catal 4(12):4254–4260. https://doi.org/10.1021/cs501169t
16. Zhou BW, Song JL, Xie C, Chen C, Qian Q, Han B (2018a) Mo-bi-cd ternary metal chalcogenides: highly efficient photocatalyst for CO_2 reduction to formic acid under visible light. ACS Sustain Chem Eng 6(5):5754–5759. https://doi.org/10.1021/acssuschemeng.8b00956
17. Wang HL, Zhang LS, Chen ZG, Hu J, Li S, Wang Z, Liu J, Wang X (2014b) Semiconductor heterojunction photocatalysts: design, construction, and photocatalytic performances. Chem Soc Rev 43(15):5234–5244. https://doi.org/10.1039/C4CS00126E
18. Zhou CG, Wang SM, Zhao ZY, Shi Z, Yan S, Zou Z (2018b) A facet-dependent schottky-junction electron shuttle in a $BiVO_4${010}-au-Cu_2O Z-scheme photocatalyst for efficient charge separation. Adv Funct Mater 28(31):1801214. https://doi.org/10.1002/adfm.201801214
19. Tu WG, Zhou Y, Zou ZG (2014) Photocatalytic conversion of CO_2 into renewable hydrocarbon fuels: state-of-the-art accomplishment, challenges, and prospects. Adv Mater 26(27):4607–4626. https://doi.org/10.1002/adma.201400087
20. Wang Y, Liu X, Han XY, Godin R, Chen J, Zhou W, Jiang C, Thompson JF, Mustafa KB, Shevlin SA, Durrant JR, Guo Z, Tang J (2020a) Unique hole-accepting carbon-dots promoting selective carbon dioxide reduction nearly 100% to methanol by pure water. Nat Commun 11(1):2531. https://doi.org/10.1038/s41467-020-16227-3
21. Cao SW, Shen BJ, Tong T, Fu JW, Yu JG (2018) 2D/2D heterojunction of ultrathin MXene/Bi_2WO_6 nanosheets for improved photocatalytic CO_2 reduction. Adv Funct Mater 28(21):1800136. https://doi.org/10.1002/adfm.201800136
22. Wu H, Kong XY, Wen XM, Chai SP, Lovell EC, Tang JW, Ng YH (2021) Metal-organic framework decorated cuprous oxide nanowires for long-lived charges applied in selective photocatalytic CO_2 reduction to CH_4. Angew Chem Int Ed 60(15):8455–8459. https://doi.org/10.1002/anie.202015735
23. Xiong XY, Mao CL, Yang ZJ, Zhang Q, Waterhouse GIN, Gu L, Zhang T (2020) Photocatalytic CO_2 reduction to CO over Ni single atoms supported on defect-rich zirconia. Adv Energy Mater 10(46):2002928. https://doi.org/10.1002/aenm.202002928
24. Sun JW, Bian J, Li JD, Zhang Z, Li Z, Qu Y, Bai L, Yang ZD, Jing L (2020) Efficiently photocatalytic conversion of CO_2 on ultrathin metal phthalocyanine/g-C_3N_4 heterojunctions by promoting charge transfer and CO_2 activation. Appl Catal B 277:119199. https://doi.org/10.1016/j.apcatb.2020.119199
25. Sayed M, Xu FY, Kuang PY, Low J, Wang S, Zhang L, Yu J (2021) Sustained CO_2-photoreduction activity and high selectivity over Mn, C-codoped ZnO core-triple shell hollow spheres. Nat Commun 12(1):4936. https://doi.org/10.1038/s41467-021-25007-6
26. Wang Y, Godin R, Durrant JR, Tang JW (2021e) Efficient hole trapping in carbon dot/oxygen-modified carbon nitride heterojunction photocatalysts for enhanced methanol production from CO_2 under neutral conditions. Angew Chem Int Ed 60(38):20811–20816. https://doi.org/10.1002/anie.202105570
27. Hu K, Li ZJ, Bai LL, Yang F, Chu X, Bian J, Zhang Z, Xu H, Jing L (2021) Synergetic subnano Ni- and Mn-oxo clusters anchored by chitosan oligomers on 2D g-C_3N_4 boost photocatalytic CO_2 reduction. Solar Rrl 5(6):2000472. https://doi.org/10.1002/solr.202000472
28. Raziq F, Sun LQ, Wang YY, Zhang X, Humayun M, Ali S, Bai L, Qu Y, Yu H, Jing L (2018) Synthesis of large surface-area g-C_3N_4 comodified with MnO_x and au-TiO_2 as efficient visible-light photocatalysts for fuel production. Adv Energy Mater 8(3):1701580. https://doi.org/10.1002/aenm.201701580
29. Wang Q, Warnan J, Rodriguez-Jimenez S et al (2020e) Molecularly engineered photocatalyst sheet for scalable solar formate production from carbon dioxide and water. Nat Energy 5(9):703–710. https://doi.org/10.1038/s41560-020-0678-6
30. Bian J, Zhang ZQ, Feng JN, Thangamuthu M, Yang F, Sun L, Li Z, Qu Y, Tang D, Lin Z, Bai F, Tang J, Jing L (2021) Energy platform for directed charge transfer in the cascade Z-scheme heterojunction: CO_2 photoreduction without a cocatalyst. Angew Chem Int Ed 60(38):20906–20914. https://doi.org/10.1002/anie.202106929
31. Wang Y, Shang XT, Shen JN, Zhang Z, Wang D, Lin J, Wu JCS, Fu X, Wang X, Li C (2020f) Direct and indirect Z-scheme heterostructure-coupled photosystem enabling cooperation of CO_2 reduction and H_2O oxidation. Nat Commun 11(1):3043. https://doi.org/10.1038/s41467-020-16742-3
32. Zhang M, Lu M, Lang ZL, Liu J, Liu M, Chang JN, Li LY, Shang LJ, Wang M, Li SL, Lan YQ (2020b) Semiconductor/covalent-organic-framework Z-scheme heterojunctions for artificial photosynthesis. Angew Chem Int Ed 59(16):6500–6506. https://doi.org/10.1002/anie.202000929
33. Bian J, Feng JN, Zhang ZQ, Li Z, Zhang Y, Liu Y, Ali S, Qu Y, Bai L, Xie J, Tang D, Li X, Bai F, Tang J, Jing L (2019) Dimension-matched zinc phthalocyanine/$BiVO_4$ ultrathin nanocomposites for CO_2 reduction as efficient wide-visible-light-driven photocatalysts via a cascade charge transfer. Angew Chem Int Ed 58(32):10873–10878. https://doi.org/10.1002/anie.201905274
34. He F, Zhu BC, Cheng B, Yu JG, Ho WK, Macyk W (2020) 2D/2D/0D TiO_2/C_3N_4/Ti_3C_2 Mxene composite S-scheme photocatalyst with enhanced CO_2 reduction activity. Appl Catal B 272:119006. https://doi.org/10.1016/j.apcatb.2020.119006
35. Huang Q, Liu J, Feng L, Wang Q, Guan W, Dong LZ, Zhang L, Yan LK, Lan YQ, Zhou HC (2020) Multielectron transportation of polyoxometalate-grafted metalloporphyrin coordination frameworks for selective CO_2-to-CH_4 photoconversion. Natl Sci Rev 7(1):1–63. https://doi.org/10.1093/nsr/nwz096
36. Zhang HB, Wang Y, Zuo SW, Zhou W, Zhang J, Lou XWD (2021) Isolated cobalt centers on $W_{18}O_{49}$ nanowires perform as a reaction switch for efficient CO_2 photoreduction. J Am Chem Soc 143(5):2173–2177. https://doi.org/10.1021/jacs.0c08409
37. Wang JW, Jiang L, Huang HH, Han ZJ, Ouyang GF (2021a) Rapid electron transfer via dynamic coordinative interaction boosts quantum efficiency for photocatalytic CO_2 reduction. Nat Commun 12(1):4276. https://doi.org/10.1038/s41467-021-24647-y
38. Wang FL, Hou TT, Zhao X, Yao W, Fang R, Shen K, Li Y (2021b) Ordered macroporous carbonous frameworks implanted with CdS quantum dots for efficient photocatalytic CO_2 reduction. Adv Mater 33(35):2102690. https://doi.org/10.1002/adma.202102690

39. Xu FY, Meng K, Cheng B, Wang SY, Xu JS, Yu JG (2020) Unique S-scheme heterojunctions in self-assembled TiO_2/$CsPbBr_3$ hybrids for CO_2 photoreduction. Nat Commun 11(1):4613. https://doi.org/10.1038/s41467-020-18350-7
40. Hu YG, Zhan F, Wang Q, Sun Y, Yu C, Zhao X, Wang H, Long R, Zhang G, Gao C, Zhang W, Jiang J, Tao Y, Xiong Y (2020) Tracking mechanistic pathway of photocatalytic CO_2 reaction at Ni sites using operando, time-resolved spectroscopy. J Am Chem Soc 142(12):5618–5626. https://doi.org/10.1021/jacs.9b12443
41. Wang Y, Wang SB, Lou XW (2019) Dispersed nickel cobalt oxyphosphide nanoparticles confined in multichannel hollow carbon fibers for photocatalytic CO_2 reduction. Angew Chem Int Ed 58(48):17236–17240. https://doi.org/10.1002/anie.201909707
42. Zhang P, Wang SB, Guan BY, Lou XW (2019) Fabrication of CdS hierarchical multi-cavity hollow particles for efficient visible light CO_2 reduction. Energy Environ Sci 12(1):164–168. https://doi.org/10.1039/C8EE02538J
43. Tang JW, Durrant JR, Klug DR (2008) Mechanism of photocatalytic water splitting in TiO_2: reaction of water with photoholes, importance of charge carrier dynamics, and evidence for four-hole chemistry. J Am Chem Soc 130(42):13885–13891. https://doi.org/10.1021/ja8034637
44. Wang XY, Wang YS, Gao MC, Shen J, Pu X, Zhang Z, Lin H, Wang X (2020b) $BiVO_4$/$Bi_4Ti_3O_{12}$ heterojunction enabling efficient photocatalytic reduction of CO_2 with H_2O to CH_3OH and CO. Appl Catal B 270:118876. https://doi.org/10.1016/j.apcatb.2020.118876
45. Wang G, He CT, Huang R, Mao J, Wang D, Li Y (2020c) Photoinduction of cu single atoms decorated on Uio-66-NH_2 for enhanced photocatalytic reduction of CO_2 to liquid fuels. J Am Chem Soc 142(45):19339–19345. https://doi.org/10.1021/jacs.0c09599
46. Wang JC, Wang J, Li NY, du X, Ma J, He C, Li Z (2020d) Direct Z-scheme 0D/2D heterojunction of $CsPbBr_3$ quantum dots/Bi_2WO_6 nanosheets for efficient photocatalytic CO_2 reduction. ACS Appl Mater Interfaces 12(28):31477–31485. https://doi.org/10.1021/acsami.0c08152
47. Chang X, Wang T, Gong J (2016) CO_2 photoreduction: insights into CO_2 activation and reaction on surfaces of photocatalysts. Energy Environ Sci 9(7):2177–2196. https://doi.org/10.1039/C6EE00383D
48. Meng AY, Zhang LY, Cheng B, Yu JG (2019) Dual cocatalysts in TiO_2 photocatalysis. Adv Mater 31:1807660. https://doi.org/10.1002/adma.201807660
49. Kong TT, Jiang YW, Xiong YJ (2020) Photocatalytic CO_2 conversion: what can we learn from conventional CO_x hydrogenation? Chem Soc Rev 49(18):6579–6591. https://doi.org/10.1039/C9CS00920E
50. Habisreutinger SN, Schmidt-Mende L, Stolarczyk JK (2013) Photocatalytic reduction of CO_2 on TiO_2 and other semiconductors. Angew Chem Int Ed 52(29):7372–7408. https://doi.org/10.1002/anie.201207199
51. Prabhu P, Jose V, Lee JM (2020) Heterostructured catalysts for electrocatalytic and photocatalytic carbon dioxide reduction. Adv Funct Mater 30(24):1910768. https://doi.org/10.1002/adfm.201910768
52. Meng XG, Ouyang SX, Kako T, Li P, Yu Q, Wang T, Ye J (2014) Photocatalytic CO_2 conversion over alkali modified TiO_2 without loading noble metal cocatalyst. Chem Commun 50(78):11517–11519. https://doi.org/10.1039/C4CC04848B
53. Fu JW, Jiang KX, Qiu XQ, Yu J, Liu M (2020) Product selectivity of photocatalytic CO_2 reduction reactions. Mater Today 32:222–243. https://doi.org/10.1016/j.mattod.2019.06.009
54. Li K, Peng BS, Peng TY (2016a) Recent advances in heterogeneous photocatalytic CO_2 conversion to solar fuels. ACS Catal 6(11):7485–7527. https://doi.org/10.1021/acscatal.6b02089
55. Li K, Peng TY, Ying ZH, Song S, Zhang J (2016b) Ag-loading on brookite TiO_2 quasi nanocubes with exposed {210} and {001} facets: activity and selectivity of CO_2 photoreduction to CO/CH_4. Appl Catal B 180:130–138. https://doi.org/10.1016/j.apcatb.2015.06.022
56. Mohamed HH, Bahnemann DW (2012) The role of electron transfer in photocatalysis: fact and fictions. Appl Catal B 128:91–104. https://doi.org/10.1016/j.apcatb.2012.05.045
57. Zhang WH, Mohamed AR, Ong WJ (2020a) Z-scheme photocatalytic systems for carbon dioxide reduction: where are we now? Angew Chem Int Ed 59(51):22894–22915. https://doi.org/10.1002/anie.201914925
58. Park H, Ou HH, Colussi AJ, Hoffmann MR (2015) Artificial photosynthesis of C1-C3 hydrocarbons from water and CO_2 on titanate nanotubes decorated with nanoparticle elemental copper and CdS quantum dots. J Phys Chem A 119(19):4658–4666. https://doi.org/10.1021/jp511329d
59. Liang L, Lei FC, Gao S, Sun Y, Jiao X, Wu J, Qamar S, Xie Y (2015) Single unit cell bismuth tungstate layers realizing robust solar CO_2 reduction to methanol. Angew Chem Int Ed 54(47):13971–13974. https://doi.org/10.1002/anie.201506966
60. Ohno T, Higo T, Murakami N, Saito H, Zhang Q, Yang Y, Tsubota T (2014) Photocatalytic reduction of CO_2 over exposed-crystal-face-controlled TiO_2 nanorod having a brookite phase with CO-catalyst loading. Appl Catal B 152:309–316. https://doi.org/10.1016/j.apcatb.2014.01.048
61. Yamamoto M, Yoshida T, Yamamoto N, Nomoto T, Yamamoto Y, Yagi S, Yoshida H (2015) Photocatalytic reduction of CO_2 with water promoted by ag clusters in ag/Ga_2O_3 photocatalysts. J Mater Chem A 3(32):16810–16816. https://doi.org/10.1039/C5TA04815J
62. Fu JW, Zhu BC, Jiang CJ, Cheng B, You W, Yu J (2017) Hierarchical porous O-doped g-C_3N_4 with enhanced photocatalytic CO_2 reduction activity. Small 13(15):1603938. https://doi.org/10.1002/smll.201603938
63. Yu JG, Wang K, Xiao W, Cheng B (2014) Photocatalytic reduction of CO_2 into hydrocarbon solar fuels over g-C_3N_4-Pt nanocomposite photocatalysts. Phys Chem Chem Phys 16(23):11492–11501. https://doi.org/10.1039/c4cp00133h
64. Albero J, Peng Y, Garcia H (2020) Photocatalytic CO_2 reduction to C2+ products. ACS Catal 10(10):5734–5749. https://doi.org/10.1021/acscatal.0c00478
65. Wang W, Deng CY, Xie SJ, Li Y, Zhang W, Sheng H, Chen C, Zhao J (2021c) Photocatalytic C-C coupling from carbon dioxide reduction on copper oxide with mixed-valence copper(I)/copper(II). J Am Chem Soc 143(7):2984–2993. https://doi.org/10.1021/jacs.1c00206
66. Zhang XJ, Han F, Shi B, Farsinezhad S, Dechaine GP, Shankar K (2012) Photocatalytic conversion of diluted CO_2 into light hydrocarbons using periodically modulated multiwalled nanotube arrays. Angew Chem Int Ed 51(51):12732–12735. https://doi.org/10.1002/anie.201205619
67. Liu X, Inagaki S, Gong JL (2016) Heterogeneous molecular systems for photocatalytic CO_2 reduction with water oxidation. Angew Chem Int Ed 55(48):14924–14950. https://doi.org/10.1002/anie.201600395
68. Gao S, Gu BC, Jiao XC, Sun Y, Zu X, Yang F, Zhu W, Wang C, Feng Z, Ye B, Xie Y (2017) Highly efficient and exceptionally durable CO_2 photoreduction to methanol over freestanding defective single-unit-cell bismuth vanadate layers. J Am Chem Soc 139(9):3438–3445. https://doi.org/10.1021/jacs.6b11263
69. Chen GB, Gao R, Zhao YF, Li Z, Waterhouse GIN, Shi R, Zhao J, Zhang M, Shang L, Sheng G, Zhang X, Wen X, Wu LZ, Tung CH, Zhang T (2018) Alumina-supported CoFe alloy catalysts derived from layered-double-hydroxide nanosheets for efficient photothermal CO_2 hydrogenation to hydrocarbons. Adv Mater 30(3):1704663. https://doi.org/10.1002/adma.201704663
70. Sharma P, Kumar S, Tomanec O, Petr M, Zhu Chen J, Miller JT, Varma RS, Gawande MB, Zbořil R (2021) Carbon nitride-based ruthenium single atom photocatalyst for CO_2 reduction to methanol. Small 17(16):2006478. https://doi.org/10.1002/smll.202006478
71. Hou WB, Hung WH, Pavaskar P, Goeppert A, Aykol M, Cronin SB (2011) Photocatalytic conversion of CO_2 to hydrocarbon fuels via plasmon-enhanced absorption and metallic interband transitions. ACS Catal 1(8):929–936. https://doi.org/10.1021/cs2001434
72. Zhuo TC, Song Y, Zhuang GL, Chang LP, Yao S, Zhang W, Wang Y, Wang P, Lin W, Lu TB, Zhang ZM (2021) H-bond-mediated selectivity control of formate versus CO during CO_2 photoreduction with two cooperative cu/X sites. J Am Chem Soc 143(16):6114–6122. https://doi.org/10.1021/jacs.0c13048
73. Du X, Zhao TY, Xiu ZY et al (2020) $BiVO_4$@$ZnIn_2S_4$/Ti_3C_2 MXene quantum dots assembly all-solid-state direct Z-scheme photocatalysts for efficient visible-light-driven overall water splitting. Appl Mater Today 20:100719. https://doi.org/10.1016/j.apmt.2020.100719
74. Pang R, Teramura K, Asakura H, Hosokawa S, Tanaka T (2017) Highly selective photocatalytic conversion of CO_2 by water over ag-loaded $SrNb_2O_6$ nanorods. Appl Catal B 218:770–778. https://doi.org/10.1016/j.apcatb.2017.06.052
75. Ran JR, Gao GP, Li FT, Ma TY, Du AJ, Qiao SZ (2017) Ti_3C_2 MXene co-catalyst on metal sulfide photo-absorbers for enhanced visible-light photocatalytic hydrogen production. Nat Commun 8(1):13907. https://doi.org/10.1038/ncomms13907
76. Gao C, Low JX, Long R, Kong TT, Zhu JF, Xiong YJ (2020) Heterogeneous single-atom photocatalysts: fundamentals and applications. Chem Rev 120(21):12175–12216. https://doi.org/10.1021/acs.chemrev.9b00840
77. Low JX, Yu JG, Jaroniec M, Wageh S, al-Ghamdi AA (2017) Heterojunction Photocatalysts. Adv Mater 29(20):1601694. https://doi.org/10.1002/adma.201601694

78. Kim C, Cho KM, Al-Saggaf A, Gereige I, Jung HT (2018) Z-scheme photocatalytic CO_2 conversion on three-dimensional $BiVO_4$/carbon-coated Cu_2O nanowire arrays under visible light. ACS Catal 8(5):4170–4177. https://doi.org/10.1021/acscatal.8b00003
79. Fu JW, Xu QL, Low JX, Jiang CJ, Yu JG (2019) Ultrathin 2D/2D WO_3/g-C_3N_4 step-scheme H_2 production photocatalyst. Appl Catal B 243:556–565. https://doi.org/10.1016/j.apcatb.2018.11.011

Publisher's Note